Reconfigurable Antennas for Wireless Communications

Yingjie Jay Guo and Pei-Yuan Qin

Contents

Abstract

With the capability to dynamically change their radiation characteristics, reconfigurable antennas will become indispensable parts for the next-generation wireless communications and sensing systems where the RF front-ends are required to be cognitive in nature. Compared to traditional antennas whose characteristics

Y.J. Guo (✉) • P.-Y. Qin
University of Technology, Sydney, Australia
e-mail: jay.guo@uts.edu.au; pyqin1983@hotmail.com

Z.N. Chen et al. (eds.), *Handbook of Antenna Technologies*,
DOI 10.1007/978-981-4560-44-3_119

are fixed, reconfigurable antennas pose new challenges to antenna researchers and designers, such as tuning the operating frequency of an antenna whilst maintaining its radiation pattern. In the last two decades, substantial progress has been made in the development of reconfigurable antennas from both academia and industry. This chapter provides an overview of the state-of-the-art of reconfigurable antennas by elaborating the basic concepts of different reconfigurable antennas and practical techniques to realize them. It is focused on both reconfigurable antenna elements and arrays, and outlines some directions for future research.

Keywords

Reconfigurable antennas • Frequency reconfigurable antennas • Polarisation reconfigurable antennas • Pattern reconfigurable antennas • Leaky wave antennas • Phase shifters • Arrays

Introduction

Owing to the rapid proliferation of wireless communications systems, the limited electromagnetic spectrum has become more and more congested. To address this challenge, future wireless communications systems need to be cognitive and reconfigurable. They will have the intelligence and capacity to adopt the most appropriate communications strategy based on the feedback from channel sensing activities and signal quality assessment, including the operating frequency, the main beam direction and modulation schemes. In order to achieve these flexibilities, reconfigurable antennas (RAs) with adaptive radiation characteristics are required instead of traditional antennas whose structures are tailored to fit particular applications. RAs can also be used to avoid interference, save energy, enhance security, and mitigate signal quality deterioration caused by multipath fading.

Typical parameters of an antenna that can be reconfigured include frequency, polarization, radiation pattern, or a combination of the above. Depending on the reconfiguration mechanisms, RAs can also be classified into three main groups, namely, those using electrical devices, such as PIN diodes, varactor diodes and radio frequency micro electromechanical system (RF-MEMS), and those using mechanical changes and using material changes. Although this topic is a relatively new one, there are several books (Bernhard 2005; Bernhard and Volakis 2007) dedicated to it and a large number of papers reported (Christodoulou et al. 2012). This chapter presents recent progress of RAs using electrical methods to achieve reconfiguration. Regarding those RAs using mechanical changes, readers can refer to (Tawk et al. 2011; Bernhard et al. 2001) for frequency RAs, (Barrera and Huff 2014) for polarization RAs and (Rodrigo et al. 2012; Sievenpiper et al. 2002) for pattern RAs.

The remainder of the chapter is organised as follows. Sections "Frequency Reconfigurable Antennas (RAs)," "Polarization Reconfigurable Antenna (RA)," "Pattern Reconfigurable Antenna (RA)," and "Compound Reconfigurable Antennas (RAs)" review the designs of frequency RAs, polarization RAs, pattern RAs and combined frequency and polarization RAs, respectively. Section "Reconfigurable

Phase Shifter and Its Application in Beamforming Antennas" describes a novel phase shifter based on reconfigurable defected microstrip structure and its application in a beam-scanning antenna arrays. Section "Reconfigurable Leaky Wave Antennas" presents some designs of reconfigurable leaky wave antennas. Section "Summary" summarizes this chapter and gives some directions for future research.

Frequency Reconfigurable Antennas (RAs)

Frequency RAs can change the antenna operating frequency while keeping the polarization and radiation pattern stable across the entire frequency tuning range. Currently, it is a common practice for a single radio device to handle several services over a wide range of frequencies. For example, smart mobile phones or laptops may be required to support different standards, such as wireless local area network (WLAN), Worldwide Interoperability for Microwave Access (WiMAX), Bluetooth, Global Positioning System (GPS), 3G and 4G. To this end, the antennas need to cover multiple frequency bands. From the antenna perspective, multiband, wideband and frequency RAs are three potential candidates to be employed in systems requiring multiple operating bands. However, if only a portion of these operating bands is required at any given time, then frequency RAs would be the most appropriate choice. Compared to multiband and wideband antennas, one of the merits of frequency RAs is that the antenna can provide noise rejection in the bands that are not in use, so that the filter requirements of the front-end circuits can be greatly reduced. Furthermore, compared to multiband or wideband antennas, frequency RAs can be made much more compact.

Frequency RAs can be classified according to the basic antenna elements employed including microstrip antennas, dipole antennas, planar inverted F antennas (PIFA) and slot antennas. Alternatively, frequency RAs can also be classified into two types, namely, frequency continuous tuning and discrete tuning. The following introduction will be presented based on this classification.

Continuous Tuning

Varactor diodes are usually employed to achieve continuous frequency tuning. Initial work in this regard employed a method to load the radiating edges of patch antennas with varactor diodes to realize frequency agility (Bhartia and Bahl 1982; Waterhouse and Shuley 1994). By changing the bias voltages of the varactor diodes, the effective electrical size of the patch can be varied, which can produce a 1.1–1.2 frequency tuning ratio. Hum et al. proposed a differentially-fed frequency-agile microstrip patch antenna (Hum and Xiong 2010), as shown in Fig. 1. By loading three pairs of varactor diodes on the microstrip patches, the antenna can achieve a 2.0 frequency tuning ratio. Microstrip slot antennas also serve as good candidates for frequency RA designs. By using varactor diodes to change the length of the slot, the frequency of

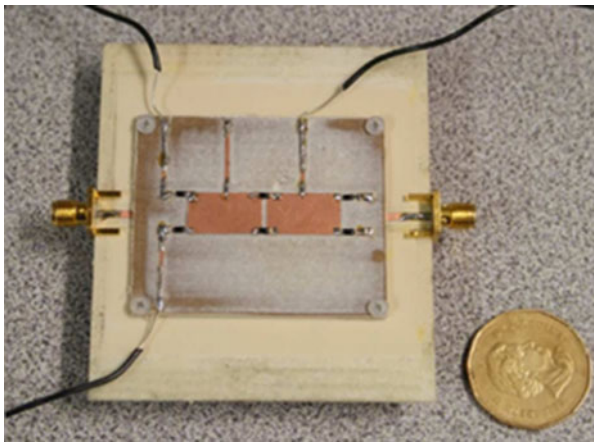

Fig. 1 Differentially-fed frequency-agile microstrip patch antenna

the antenna can be tuned. Generally speaking, slot frequency RAs can accomplish a wider tuning ratio, such as 3.52 (Li et al. 2010a), but they have the drawbacks of lower gain and efficiency.

Owing to the advantages of high gain, wide impedance bandwidth and ease of integration with microstrip-based monolithic-microwave integrated-circuits (MMIC), frequency reconfigurable printed quasi-Yagi dipole antennas have attracted significant attention (Deal et al. 2000). Compared to a broadband printed dipole antenna with fixed frequency response, a frequency reconfigurable design offers frequency selective functionality which can reduce the adverse effects of co-site interference and jamming. The mechanism of frequency reconfiguration is to change the electrical length of the dipole arms by using varactor diodes or switches. In (Cai et al. 2012), a frequency reconfigurable high-gain quasi-Yagi dipole antenna operating over the 478–741 MHz UHF TV band was proposed for cognitive radio applications. The antenna consists of two main parts: a printed Yagi antenna with varactor-loaded dipole elements and a metallic corner reflector combined with a metallic hollow box for mechanical support, as shown in Fig. 2. The antenna metallization is etched on both sides of a Rogers RO3035 printed circuit board (PCB) with dimensions of 745 mm $\times$ 360 mm. The thickness of the substrate is 1.524 mm and the dielectric constant is 3.55. The top metallization consists of a driven dipole element, four parasitic directors, a broadband microstrip-to-coplanar stripline (CPS) transition and resistive biasing lines. The bottom side is a truncated microstrip ground, which serves as the reflector element for the antenna. Two varactor diodes are placed in each arm of the driven dipole and in each director. As the capacitance of the varactor diodes in the driven dipole is varied, the effective length of the dipole is changed, thereby altering the antenna resonant frequency. In the meantime, the varactor diodes in the directors are tuned to maximise the gain and to realize an acceptable impedance match for each operating frequency. A simulated and measured frequency tuning range from 478 to 741 MHz is achieved, which is

Fig. 2 Photo of the frequency reconfigurable UHF antenna (with a 60 cm long metallic ruler)

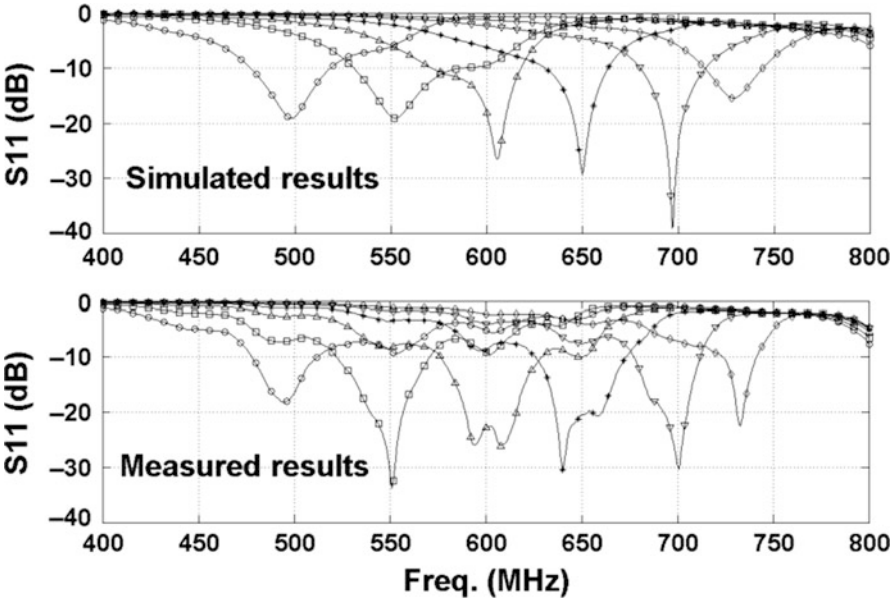

Fig. 3 Simulated and measured reflection coefficients in the six tuning sub-bands

shown in Fig. 3. In order to bias the diodes embedded in the driver and directors that are located on the ungrounded substrate, a low-cost and effective resistive biasing circuitry is employed, in which thin (1 mm width) but long metallic strip lines are broken down in short sections. The gaps between the metallic sections are bridged with high value surface mount resistors. The resistive nature of the biasing circuitry chokes high frequency currents effectively.

Discrete Tuning

PIN diode and MEMS switches are usually employed to realize discrete frequency tuning. A typical example is the compact frequency-agile microstrip patch antenna presented in (Genovesi et al. 2014). The antenna consists of a central patch connected to four different peripheral elements using PIN diodes. Each one of the four peripheral elements operates at a certain frequency independent from the others that can be designed according to the specifications. The patch antenna can achieve an overall of $2^4 = 16$ different states within a wide frequency range from 0.8 to 3.0 GHz.

In addition, a frequency reconfigurable folded dipole quasi-Yagi antenna was presented in (Qin et al. 2010b). The antenna is printed on two sides of a RO4003 substrate (0.813 mm thick and dielectric constant 3.55). The configuration of the antenna is shown in Fig. 4. The top side of the substrate consists of a microstrip feed, a broad-band microstrip-to-CPS balun, a folded dipole driver element fed by the CPS

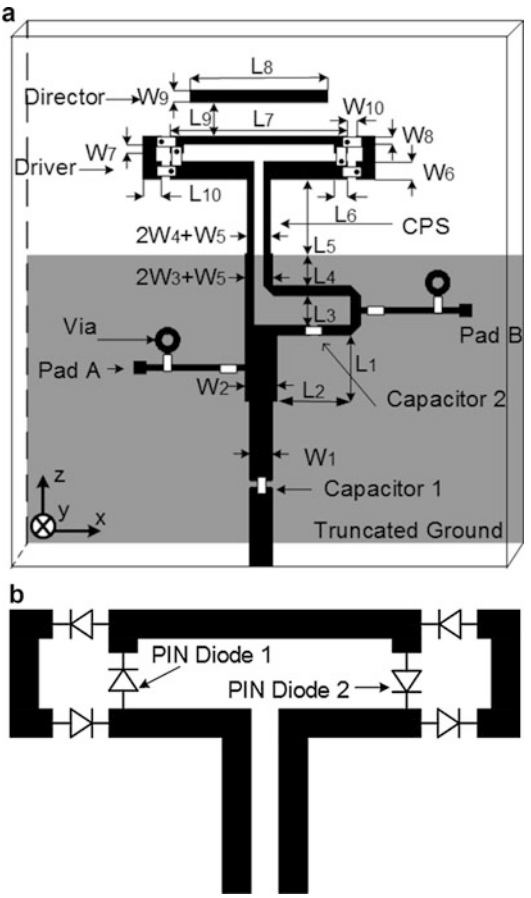

Fig. 4 (**a**) Configuration of the reconfigurable quasi-Yagi folded dipole Antenna. (**b**) Orientation of the PIN diodes in the folded dipole

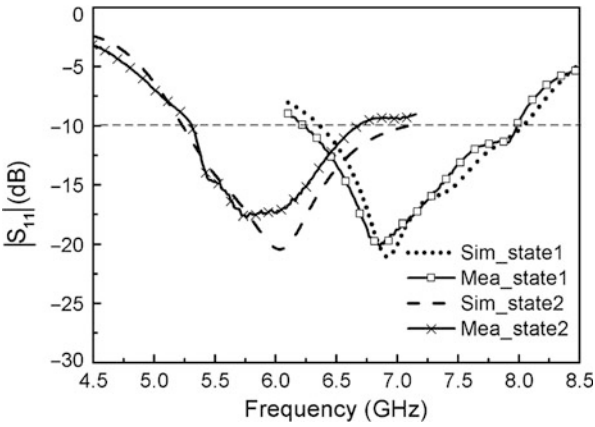

Fig. 5 Simulated and measured input reflection coefficients for the different states of Antenna

and a dipole parasitic director element. The bottom side is a truncated microstrip ground serving as the reflector element for the antenna. The combination of the parasitic director and reflector element directs the radiation of the antenna towards the end-fire direction. The folded dipole driver element is printed with six 0.5 mm gaps. Six PIN diodes are mounted across the gaps using electrically conductive silver epoxy. The length of the folded dipole element can be changed by switching between the different states of the diodes. When diodes 1 and 2 are on and all the other diodes are off, the length of the folded dipole is L_7. In this case, the length of the folded dipole is short and the proposed antenna resonates at a high operating frequency (denoted as State I). Changing the polarity of the dc voltage turns diodes 1 and 2 off and all the other diodes on. In this case, the length of the folded dipole is increased to $L_7 + 2\,W_{10} + 2\,L_{10}$ and the antenna resonates at a lower frequency (denoted as State II). Figure 5 shows the simulated and measured reflection coefficients versus frequency for State I and State II. From State II to State I, the resonant frequency shifts from 5.95 to 7.2 GHz, corresponding to a frequency ratio of 1.21. The dc bias voltages are applied to the diodes through the metallization of the balun, CPS and folded dipole. It can be noted that, by using a folded dipole, a closed dc circuit is formed, thereby eliminating the need for extra biasing lines to be attached to the folded dipole. This, in turn, helps maintain the radiation pattern across the frequency tuning range.

Polarization Reconfigurable Antenna (RA)

Polarization reconfiguration can take place in the form of changing angles of linear polarizations, or switching between left-hand circular polarization (LHCP) and right-hand circular polarization (RHCP), as well as between linear and circular polarizations. Such antennas can provide polarization diversity to mitigate signal fading in multipath propagation environments. Moreover, polarization diversity can be employed to increase the capacity of a multiple-input-multiple-output (MIMO)

system (Qin et al. 2010a, b). The main challenge in achieving polarization agility is that it must be accomplished without significant changes in the antenna input impedance characteristics. As a result, it is challenging to design a polarization RA that can switch between linear and circular polarizations because it is difficult to simultaneously realize a good impedance match for these two polarizations. The reason is that circular polarization (CP) is typically generated by two degenerate orthogonal linear modes, and its input impedance is significantly different from that of the one resonant mode used to generate linear polarization (LP). Furthermore, it is even more difficult to design a dual-band or a multi-band polarization RA as the interdependence between the frequency response and the polarization characteristic is much stronger than that of a single-band antenna. In other words, it is more challenging to change the polarization states for the dual/multiple bands simultaneously while keeping the frequency response stable. In this section, some novel techniques are presented that can realize polarization switching between linear and circular senses and dual-band polarization RAs.

Single Band Polarization RA

Several interesting polarization RA designs have been proposed to switch between circular and linear polarizations. In (Sung et al. 2004), four pin-diodes were used on a corner-truncated square patch to produce LP and CP radiation with a small impedance bandwidth (2.5 %). A perturbed square-ring slot antenna using four pin diodes was designed that allows operation in both CP and LP modes (Dorsey and Zaghloul 2009). Unfortunately, the authors did not introduce the physical biasing and control circuits. In (Chen and Row 2008), a ring-slot-coupled microstrip circular patch antenna, as shown in Fig. 6, was proposed that can switch between linear and circular polarizations with an overlapped impedance bandwidth of 2.2 %. It was fabricated on two single FR4 substrates separated by a piece of foam, thus it may be difficult to integrate the antenna into a compact wireless device due to its large volume.

Another example is the design of a microstrip U-slot patch antenna that can switch between linear and circular polarizations (Qin et al. 2010c). The configuration of the proposed antenna is shown in Fig. 7. A U-slot is inserted into a rectangular patch which is printed on a 3.175-mm-thick RT/duroid 5880 substrate (dielectric constant 2.2). It should be noted that in the antenna prototype, another thinner slot is cut on the top of the U-slot, which separates the patch into two parts to ensure dc isolation. Three 30 pF capacitors are placed across this thinner slot to maintain RF continuity. The outer part of the patch is dc grounded by a shorting pin through an inductor used as an RF choke. Both the dc bias voltage and the RF signal are simultaneously fed through the coaxial probe by using a bias-tee. Beam lead PIN diodes are used as switching elements in the U-slot. The length of the U-slot arm can be changed by changing between the different states of the diodes. When the left diode is on and the right diode is off, the RF current can flow across the left arm of the U-slot. In this case, the left arm of the U-slot is shorter than the

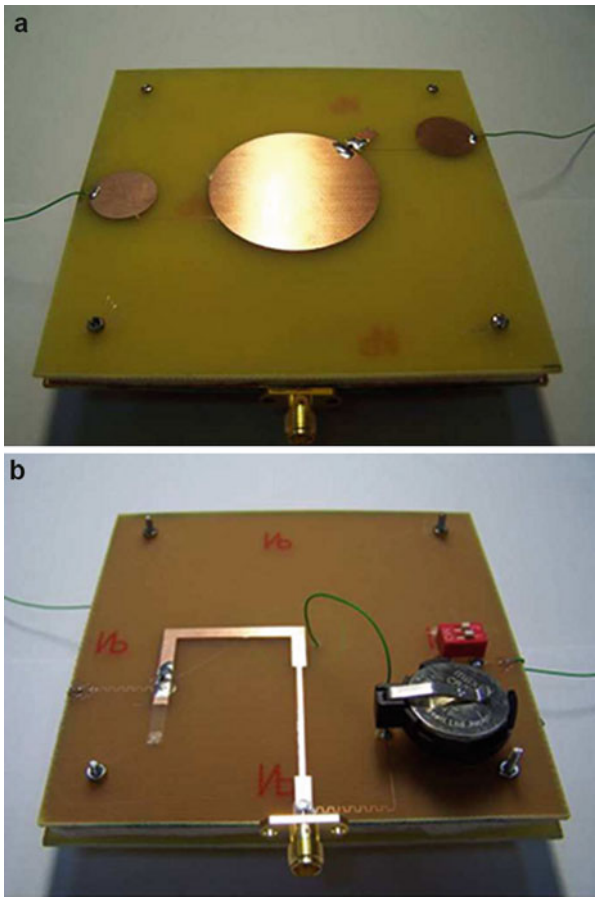

Fig. 6 Circular patch polarization reconfigurable antenna: (**a**) Top layer; (**b**) Bottom layer

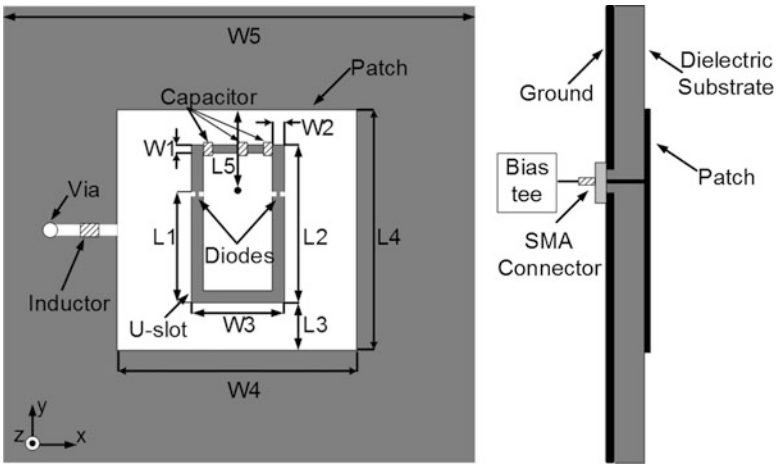

Fig. 7 Schematics of the reconfigurable U-slot antenna

right arm. The asymmetrical U-slot can excite two orthogonal modes in the patch. Adjusting the location of the PIN diodes can make the two modes have the same magnitude and a phase difference of 90° at a given frequency, thus enabling the antenna to generate CP radiation with an acceptable axial ratio. The antenna radiates LHCP when the left arm of the U-slot is longer than the right arm. RHCP can be achieved if the right arm is longer than the left arm. The U-slot becomes symmetrical when both of the diodes are on or off, which enables the antenna to radiate linear polarization. In this case, the electric field polarization is parallel to the y-axis in Fig. 7.

Simulated and measured input reflection coefficients versus frequency for the CP and LP modes are shown in Fig. 8a. Simulated and measured axial ratios at boresight for the CP mode are given in Fig. 8b. From the experimental results, it is observed that the impedance bandwidths for the LP and CP modes are 6.1 % and 13.5 %, respectively, with almost the same center frequency of 5.9 GHz, which can cover the entire 5.725–5.85 GHz wireless local area network (WLAN) band. The measured 3 dB axial ratio bandwidth at boresight extends from 5.7 to 5.86 GHz (2.8 %).

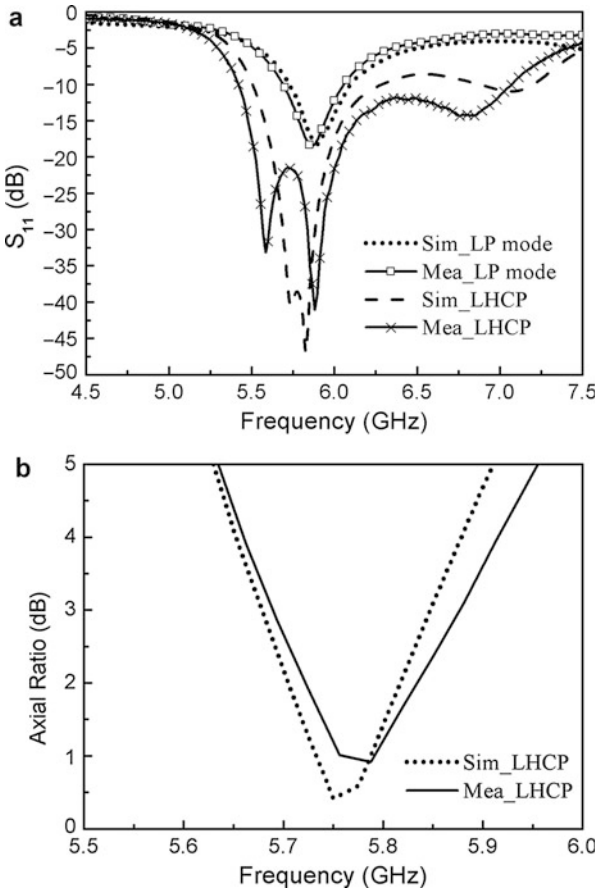

Fig. 8 Simulated and measured (**a**) input reflection coefficients for the LP and CP modes (**b**) axial ratio for the CP mode

Dual-band Polarization RA

Recently, many single-band polarization reconfigurable antennas have been developed for WLAN systems. Hsu et al. designed a polarization reconfigurable microstrip antenna using piezoelectric transducers (PETs) (Hsu and Chang 2007). Either RHCP or LHCP can be obtained by changing the bias voltage of two PETs at 5.8 GHz. An E-shaped patch antenna was studied in (Khidre et al. 2013), which is capable of radiating either RHCP or LHCP targeting the 2.4 GHz band. Li et al. described a microstrip square slot antenna with a coplanar waveguide-to-slot line transition (Li et al. 2010b). It can switch between horizontal and vertical polarizations at 2.4 GHz. For the above reported designs, the antennas can reconfigure their polarizations at only one frequency band of the WLAN standards. Since dual-band operation is commonplace for today's WLAN devices, a polarization reconfigurable antenna operating at both 2.4 and 5.8 GHz bands is highly desirable. To meet this requirement, Qin et al. proposed a single-aperture-fed polarization reconfigurable antenna enabling the switch between horizontal, vertical, and 45° linear polarizations in both 2.4 and 5.8 GHz bands (Qin et al. 2013a).

The configuration of the proposed antenna is shown in Fig. 9. The antenna consists of two substrate layers as shown in Fig. 9a, b, respectively. A side view of the antenna structure is given in Fig. 9c. The first layer is a 4.75-mm-thick RT/Duriod 5880 substrate (dielectric constant 2.2). A square patch inserted with four shorting posts is printed on the top side of this layer. There is no metallization on the bottom side of this layer. The TM_{10} and TM_{30} modes of the microstrip patch are selected to make the antenna operate in the 2.4 and 5.8 GHz bands, respectively. Generally speaking, the resonant frequency of TM_{30} mode is three times as high as that of TM_{10} mode. In order for the frequency ratio of the two modes to meet the WLAN dual-band (2.4 and 5.8 GHz) requirement, shorting posts are inserted at the nulls of the electric field of the TM_{30} mode. The shorting posts have a significant effect on the resonant frequency of TM_{10} mode whilst having little effect on the TM_{30} mode. In this way, the frequency gap between the two modes is reduced.

The second layer is a 1.524-mm-thick RO4003C substrate (dielectric constant 3.55) with metallization on both sides. On the top side, a modified H-shaped feed aperture consisting of an ordinary H-shaped slot and a smaller centrally located square slot are etched in the ground plane (see Fig. 9b). The patch is coupled to the microstrip feed line through this aperture. The dimensions of the modified H-shaped aperture are optimized to achieve good impedance match for each polarization state of the dual bands. A 50-Ω-microstrip feed line (blue dashed line in Fig. 9b) is printed on the bottom side of this layer.

As the microstrip feed line is located along the diagonal line of the patch, both the *x* - and *y*- polarized modes with the same resonant frequency are excited for both TM_{10} and TM_{30} modes. By connecting the middle of the patch edges α (Fig. 9a) to the ground through metallic vias, the resonant frequency of the *y*-polarized mode is changed without affecting the *x*-polarized mode. This is

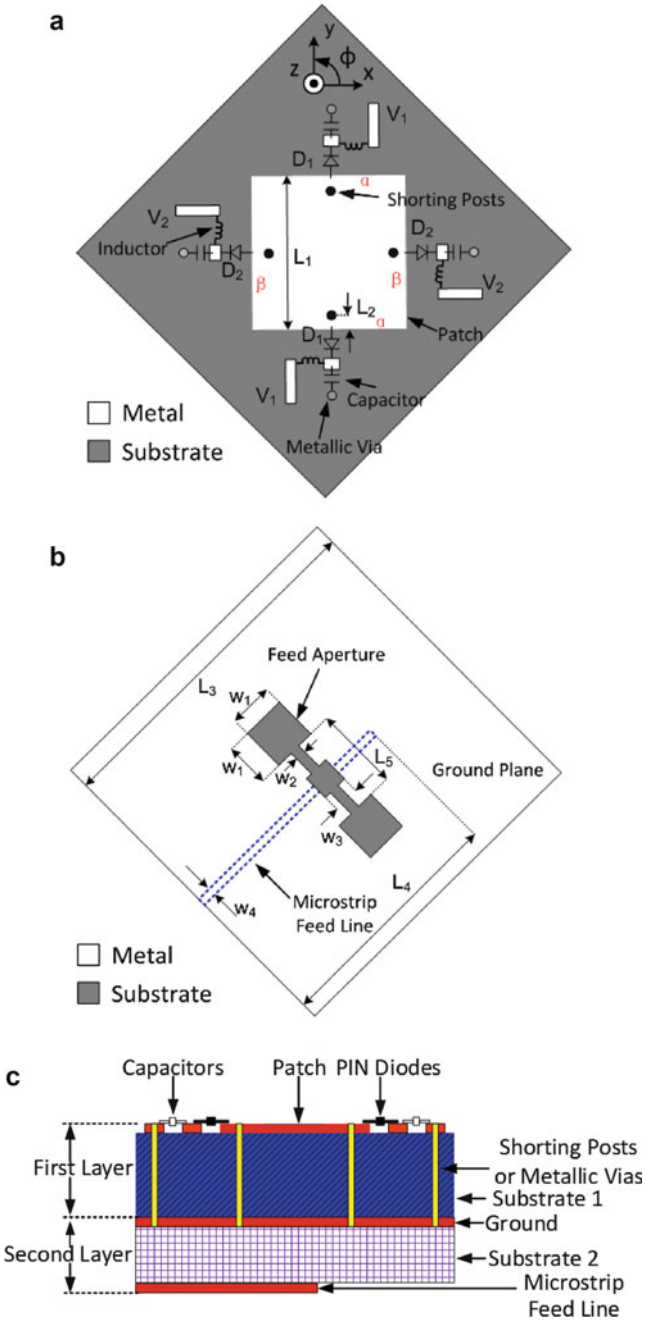

Fig. 9 Schematics of the proposed antenna: (**a**) First layer; (**b**) Second layer; (**c**) Side view

because edges α are the radiating edges for the *y*-polarized mode. Similarly, by shorting the middle of the patch edges β to the ground, the resonant frequency of the *x*-polarized mode is changed without affecting the *y*-polarized mode. Therefore, a single mode (*x*- or *y*- polarized) can be selected by shifting the resonant frequency of another mode away from targeted bands. For the proposed antenna, PIN diodes are placed between the vias and the middle of each patch edge so that the connection between the patch edges and ground can be controlled. According to the orientation of the PIN diodes in Fig. 9a, the edges α of the patch are shorted to the ground when PIN diodes D1 are turned on and D2 are turned off. In this case, the frequency of *y*-polarized mode is shifted to above the *x*-polarized one. The *x*-polarized one is chosen as the antenna operating mode (State I). When PIN diodes D1 are turned off and D2 are turned on, the *y*-polarized mode is chosen as the antenna operating mode (State II). When all the diodes are turned off, the antenna radiates 45° linear polarization (State III) that is parallel to the feed line. When all the diodes are switched on, it is found that the input reflection coefficient of the antenna is too high to be acceptable for WLAN applications.

Figures 10, 11 and 12 show the simulated and measured input reflection coefficients versus frequency for States I, II and III, respectively. It can be observed that for States I and II two bands are found at 2.4 and 5.8 GHz. As discussed in last paragraph, the mechanism of the polarization reconfiguration is to separate the *x*- and *y*-polarized modes by moving the resonant frequency of one mode away from the targeted bands. As a result, in Figs. 10 and 11, it can be seen that the undesired modes are around 2.7 GHz. In addition, for the three polarization states, there is a parasitic resonance around 3.8 GHz, which is caused by the feed aperture. In practice, filters would be employed in a wireless communications system to reject the interference signals from the unwanted frequency bands.

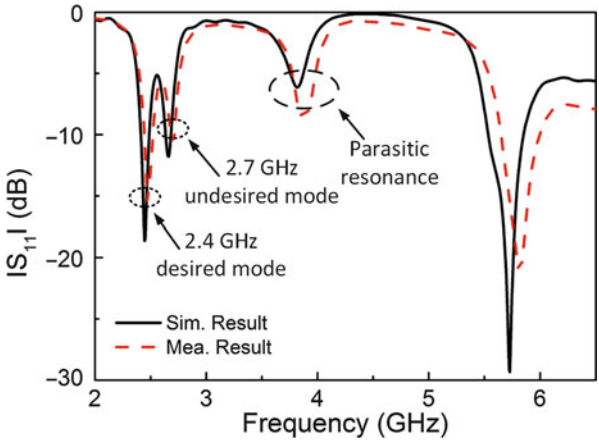

Fig. 10 Simulated and measured input reflection coefficients for State I (*x*-oriented polarization)

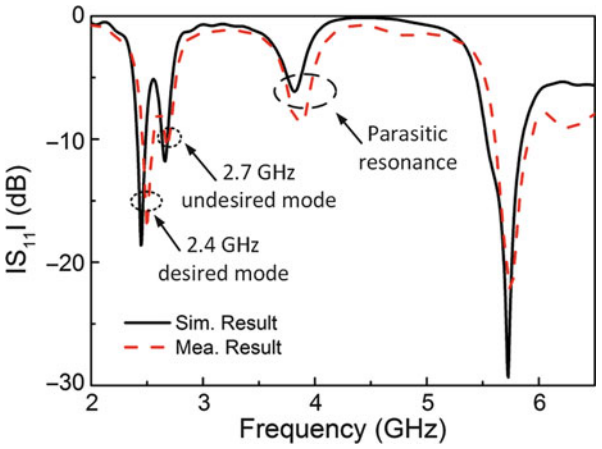

Fig. 11 Simulated and measured input reflection coefficients for State II (*y*-oriented polarization)

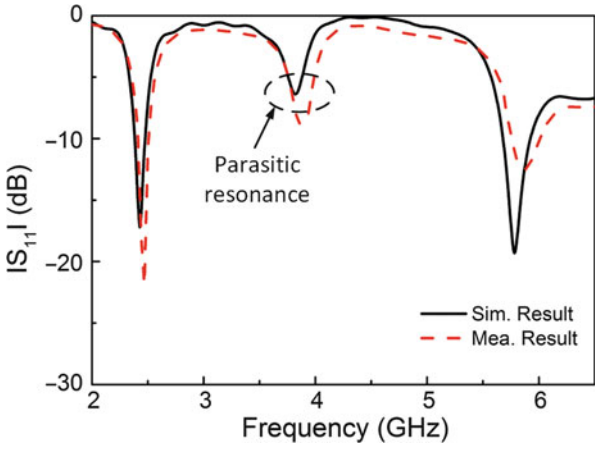

Fig. 12 Simulated and measured input reflection coefficients for State III (45^0-oriented linear polarization)

Pattern Reconfigurable Antenna (RA)

Pattern RAs have the capability to change the main-beam shape or provide main-beam scanning. They have the potential to reduce interference by altering the null positions, to save energy by directing the signal toward intended users and to provide large coverage by steering the main beam. In addition, pattern diversity provided by pattern reconfigurable antennas can be exploited by the multiple-input-multiple-output (MIMO) systems to increase the system capacity and/or link quality.

The frequency characteristic should be maintained nearly unchanged for the different radiation patterns of the antenna. Since the currents on the antenna structure directly determine the antenna radiation pattern, the reconfigurability of the radiation pattern is usually realized by manipulating the current distribution. However, as the current distribution also has a strong impact on the antenna frequency response, it is very

challenging to deliver pattern reconfigurability without significant changes in the operating frequency. Several methods have been employed to overcome this challenge. One of them is to use specific antenna structures, such as reflector antennas or parasitically coupled antennas, so that the input feed port can be almost independent from the reconfigured part of the structure, allowing frequency characteristics to remain almost stable. Another measure is to compensate for the changes in the antenna input impedance by using some additional structures or matching circuits.

Change of Main-Beam Shape

An example is a wideband circular patch antenna that can switch between boresight and conical radiation patterns by using dual L-probe feeds (Yang and Luk 2006). TM_{11} mode for boresight radiation and TM_{01} for conical radiation are excited by the two feeds, respectively. Four shorting posts are added to the patch to reduce mainly the resonant frequency of the conical pattern mode, thereby enlarging the overlapped operating frequency of the two modes. In order to reconfigure the radiation pattern electronically, an integrated matching network consisting of switches is required. In (Wu and Ma 2008; Li et al. 2011), wideband bow-tie pattern reconfigurable antennas with tunable coplanar waveguide (CPW)-to-Slotline transition feed were presented. PIN diodes are used to reconfigure the feed mode between CPW mode, left slotline (LS) mode, and right slotline (RS) mode. The CPW feed mode can generate an almost omni-directional pattern while the LS mode and the RS mode can excite two end-fire patterns whose main beams are directed to exactly opposite directions.

Another example is a pattern reconfigurable U-slot antenna that is shown in Fig. 13 (Qin et al. 2012). A U-slot is inserted into a square patch of dimensions $L1 \times L1$ on a 3.175-mm-thick RT/Duroid 5880 substrate (dielectric constant 2.2). Each side of the patch is connected with two shorting posts via PIN diodes. The orientation of the diodes is also shown in Fig. 13. As all PIN diodes are mounted across the ground and the center patch, only a bias tee attached to the SMA connector is needed to control the PIN diodes. When the bias voltage is supplied from the coaxial probe, opposite bias conditions are applied to diodes in group A and B due to their reversed orientation. When the dc voltage is zero, all diodes are turned off. In this case, the antenna operates in the normal patch mode and radiates a boresight pattern (State I). When the dc voltage is negative, diodes in group B are on, and the other diodes are off. In this case, the antenna has four shorting posts connected and can be regarded as a monopolar patch antenna, which radiates a conical pattern with the maximum power level in the *z*-*y* plane (State II). Changing the polarity of the dc voltage from negative to positive, diodes in group A are on, and all the other diodes are off. In this case, a similar conical pattern can be observed with the maximum power level in the *z*-*x* plane (State III). Two shorting posts are used at each side of the patch instead of one in order to realize good impedance match for all operating states.

Simulated and measured normalized radiation patterns at 5.3GHz for the *z*-*x* and *z*-*y* planes are displayed in Figs. 14 and 15, respectively. For State I, boresight radiation patterns with a maximum cross-polarization level of −20 dB are shown in

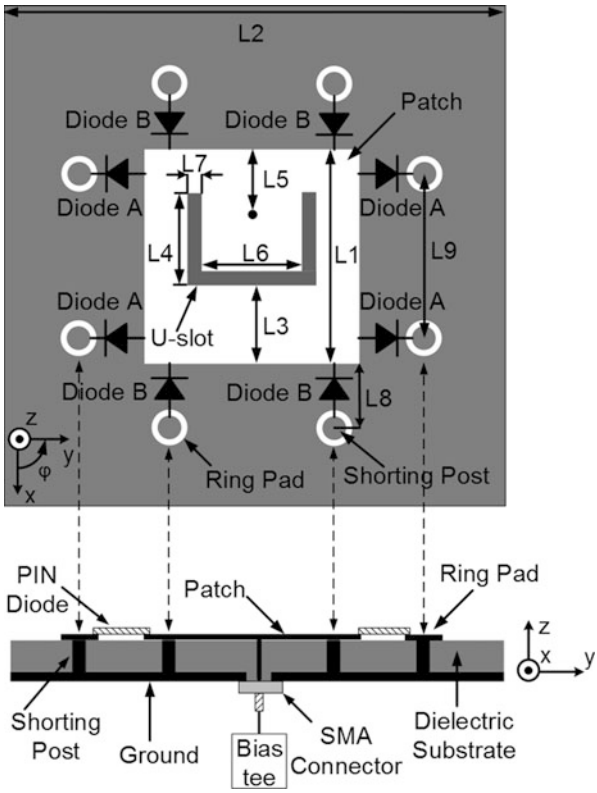

Fig. 13 Schematics of the pattern reconfigurable U-slot antenna

Figs. 14a and 15a. For State II, a symmetrical conical pattern with the maximum power level in the *z*-*y* plane directed at (elevation angle) 44° is plotted in Figs. 14b and 15b. For State III, an asymmetrical conical pattern with the maximum power level in the *z*-*x* plane directed at (elevation angle) 45° is drawn in Figs. 14c and 15c. It can be seen from Fig. 14c that the pattern is asymmetrical and there is 1 dB difference between the left and right maximum power level of the conical pattern. This is due to the position of the probe feed. Simulation results show that if the probe feed is located at the center of the patch, the difference between the left and right maximum power level in Fig. 14c will become smaller. However, in that case the overlapped impedance bandwidth of the two modes will be reduced. This can be viewed as a compromise for the antenna to provide good overlapped impedance bandwidth and radiation patterns.

Main Beam Scanning

Various antennas have been proposed to steer the main beam to predefined directions by using electronic switches, such as PIN diodes, to activate one or several elements out of a few radiators. Lai et al. proposed a four-element L-shaped antenna array that can

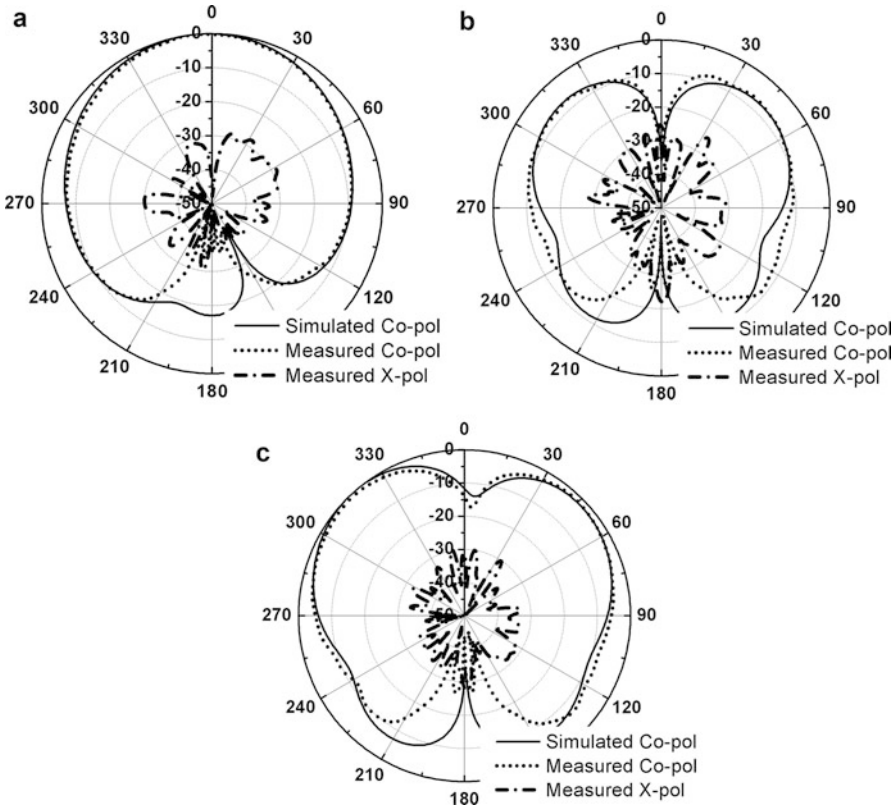

Fig. 14 Measured and simulated *z-x* plane normalized radiation patterns of the proposed antenna at 5.3 GHz (**a**) State I (**b**) State II (**c**) State III

achieve beam steering over 360^0 in the azimuth plane with a gain around −0.5–2.1 dBi (Lai et al. 2008). The configuration of the antenna is shown in Fig. 16. It is composed of four L-shaped quarter-wavelength slot antenna elements which are arranged towards 0^0, 90^0, 180^0, and 270^0, respectively. The maximum radiation direction is toward near the direction of the open end of the slot. As a result, by using PIN diodes to enable one or more L-shaped slot antennas, several switchable patterns can be achieved. Also, spiral structure was employed to change the main beam direction by altering the length of the spiral. In (Jung et al. 2006; Huff et al. 2003; Nair and Ammann 2007), rectangular single-arm spiral antennas were designed to change the main beam over five directions, three directions and four directions, respectively. The gains of the antennas in (Jung et al. 2006; Huff et al.2003; Nair and Ammann 2007) are between 3–6 dBi, 4 dBi, and 1.1–4.6 dBi, respectively. In addition, work has gone into developing beam-steering antennas based on Yagi-Uda type array. Usually, such antennas have one driven element and several parasitic elements integrated with switches. By controlling the switches, the directive and reflective roles of the parasitic elements can be changed, thereby changing the main beam direction. The driven element can be either a

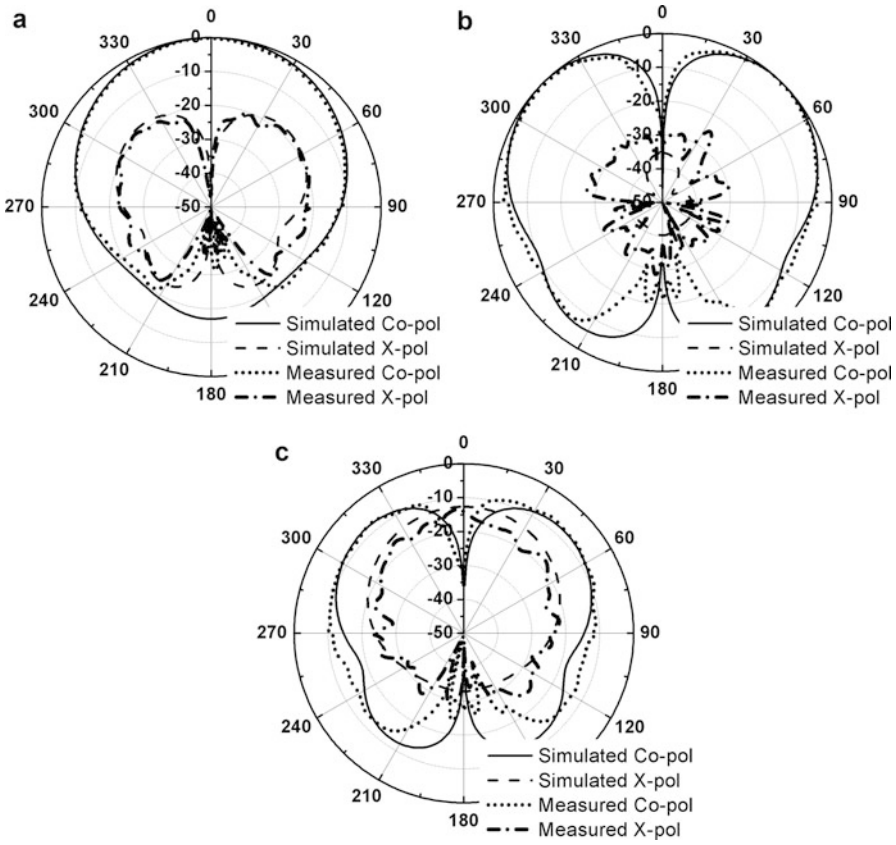

Fig. 15 Measured and simulated *z*-*y* plane normalized radiation patterns of the proposed antenna at 5.3 GHz (**a**) State I (**b**) State II (**c**) State III

microstrip dipole (Zhang et al. 2004), a microstrip patch (Yang et al. 2007; Donelli et al. 2007), or a wire antenna (Lim and Ling 2007). While there have been substantial advances in the design of beam-steering pattern reconfigurable antennas, it is found that most of the reported antennas suffer from low realized gain, which may significantly limit their applications.

In (Qin et al. 2013b), a high gain beam-switching pattern reconfigurable quasi-Yagi dipole antenna was proposed. It is capable of directing the E-plane main beam direction towards either 20^0, -20^0, or 0^0 with a realized gain between 7.5 and 10 dBi. The antenna was etched on a 1.27-mm-thick Rogers 6010 substrate (dielectric constant 10.9), as shown in Fig. 17. As shown in Fig. 17a, the top side of the substrate consists of a microstrip feed, an impedance transformer, a broad-band microstrip-to-coplanar stripline (CPS) balun, a dipole driver fed by the CPS, and two tilted rows of directive strips. The bottom side is a truncated ground, serving as the reflector. Usually, a design for maximizing the gain of a Yagi-Uda antenna requires a non-uniform director length and spacing. In this work, the directive strips

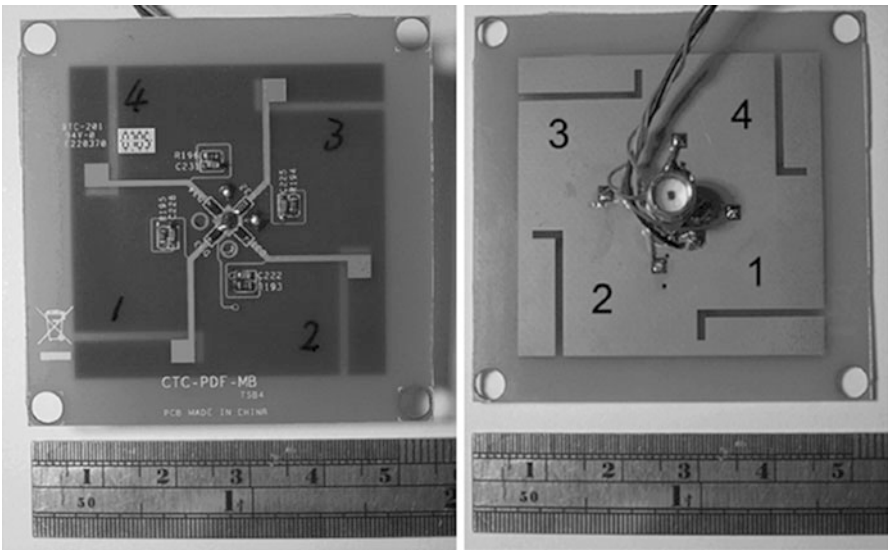

Fig. 16 L-shaped slot pattern reconfigurable antenna

are of the same length and the spacing between two adjacent strips is identical in order to reduce the design complexity.

The microstrip-to-CPS balun is used to introduce a phase difference for the currents on the two arms of the dipole. Details of the balun are shown in Fig. 17b. It can be seen that the balun is a symmetrical structure with respect to the line AA′. Therefore, only the balun above the line AA′ is described. The right-hand part of the balun is split into three sections with lengths of L_1, L_2, L_3, respectively, and the left-hand part is split into two sections with lengths of L_1 and L_4, respectively. The gap between each section is connected by PIN diodes. The width of the gap for the PIN diodes is W_{PIN}. In addition, the second section of the right-hand part of the balun with the length of L_2 is split into two smaller sections by a capacitor with a gap W_c. This capacitor is used for biasing purpose.

Conventionally, the directors of a quasi-Yagi dipole antenna are placed horizontally (parallel to the dipole driver) to direct the maximum beam towards the end-fire direction ($\varphi = 0^0$). However, it is found that when the beam is steered away from the end-fire direction, the original horizontally located directors can reduce the beam scanning range and the antenna gain. This is because the directors are not parallel to the titled beam direction any more. In order to increase the beam steering range and maintain the antenna gain, two tilted rows of metal strips are placed in front of the dipole driver with 6 strips on each row, which is shown in Fig 17a. To a certain extent, the tilted angle of the directive strips determines the maximum steering range. In this work, it is made to be close to the desired antenna beam tilted angle. Furthermore, a small gap is etched on each strip to split it into two short parts with PIN diodes inserted into the gaps. When the PIN diodes are switched on, the two short strips are connected to perform as a director. When the PIN diodes are switched

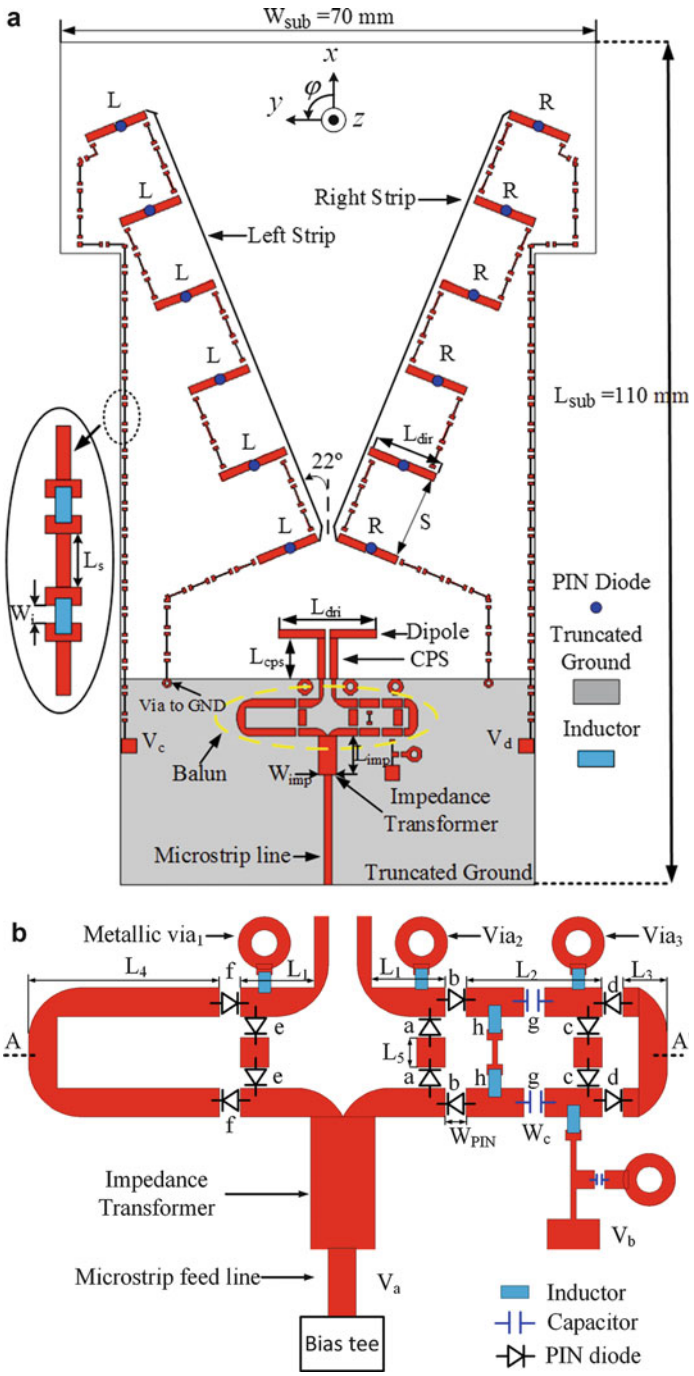

Fig. 17 Schematics of the proposed antenna: (**a**) Whole structure; (**b**) Balun of the antenna

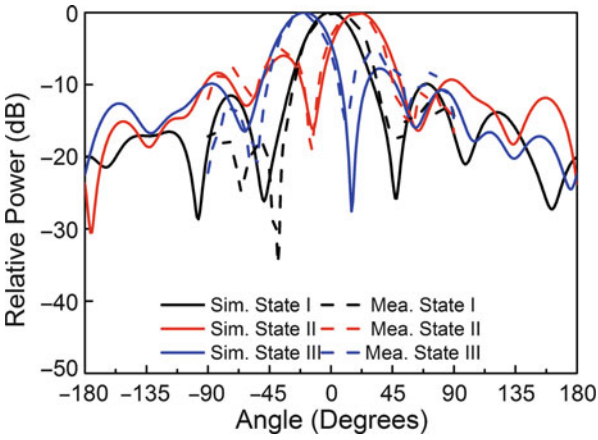

Fig. 18 Simulated and measured E-plane normalized radiation patterns at 5.2 GHz

off, the two short strips are disconnected and they do not serve as directors, thereby having little effect on the far-field radiation pattern. In this way, the PIN diodes can be used to choose the proper directors for a certain main beam direction. To be specific, when the PIN diodes *L* are switched on and the diodes *R* are switched off, only the left-hand row of strips perform as directors and they facilitate the beam tilt towards the left-hand side with respect to the end-fire direction. Similarly, when the PIN diodes *R* are switched on and diodes *L* are switched off, the beam tilt towards the right-hand side is enhanced. When both sides of the diodes are switched on, two rows of directors maintain the beam towards the end-fire direction.

By switching between the different states of the PIN diodes on the balun, the lengths of the current path on the right-hand and left-hand parts of the balun can be changed, thereby altering the phase difference of the currents on the dipole arms. According to the PIN diodes orientation shown in Fig. 17b, the antenna can operate in three states. For State I, diodes *e*, *b*, *c* and the diodes on the two rows of directive strips (diodes *L* and *R*) are switched on, and all the others are switched off. In this case, the maximum beam directs at $\varphi = 0^\circ$ (end-fire direction). For State II, diodes *e*, *b*, *d* and the diode group *L* are on, and all the others are off. In this case, the maximum beam in E plane (*x*-*y* plane) radiate towards $\varphi = 20^\circ$ direction. For State III, diodes *f*, *a*, and diode group *R* are on, and all the others are off. For this state, the maximum beam direction can be directed towards $\varphi = -20^\circ$. Figure 18 shows the simulated and measured far-field radiation patterns at 5.2 GHz. As seen from the figure, the measured main beam for State I is pointed at end fire direction, while it is steered to 19^0 and -20^0 for State II and State III, respectively.

Compound Reconfigurable Antennas (RAs)

Compound RAs have the ability to independently change the operating frequency, polarization, and radiation pattern of an antenna, which is the ultimate goal of reconfigurable antenna design. Since a compound RA can deliver more flexibility

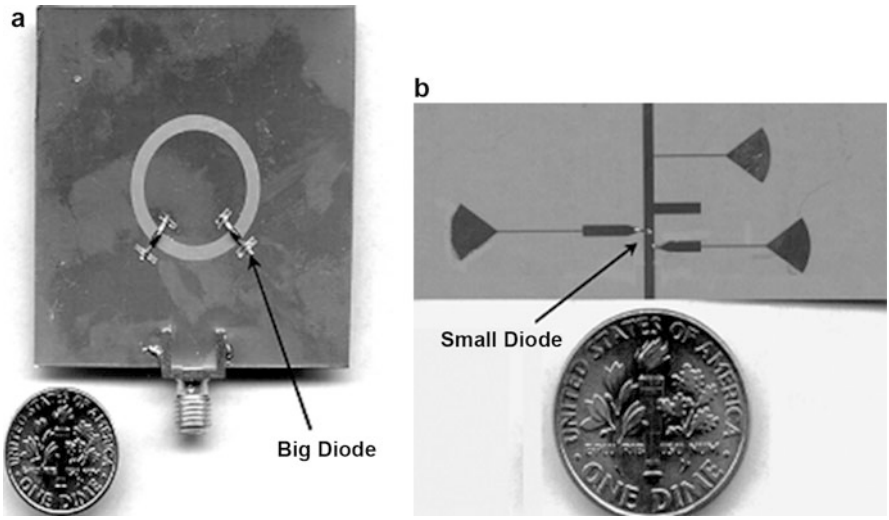

Fig. 19 (**a**) Front side of the annular slot antenna; (**b**) Back side, the impedance matching network

and diversity than a single characteristic reconfigurable antenna, it can bring significant benefits to wireless communication systems. Recently, Nikolaou et al. have achieved combined frequency and radiation pattern reconfigurability (Nikolaou et al. 2006). Figure 19 shows the antenna configuration. By loading PIN diodes across the slot at specific locations (Fig. 19a), the direction of the null of the radiation pattern can be changed. In addition, by reconfiguring the matching network shown in Fig. 19b, the operating frequency of the antenna can also be tuned.

In addition, Qin et al. proposed a single-fed combined frequency and polarization reconfigurable microstrip patch antenna with a maximum 1.67 frequency tuning ratio (Qin et al. 2011). The antenna can radiate one of the three linear polarizations (horizontal, vertical, and 45^0 linear polarizations) with a wide independent frequency tuning range for each polarization. The layout of the antenna is shown in Fig. 20. The lengths of the square substrate and the patch are 70 mm and 34 mm, respectively. The feed point is located 9 mm from the bottom of the patch edge along the diagonal line. The centre of each edge of the patch is connected to a shorting post via a PIN diode. Two varactor diodes (with a 0.1–1.0 pF junction capacitance tuning range for a corresponding voltage from 20 to 2 V) are located beside the PIN diode at each edge.

A square patch antenna fed along the diagonal line without any connection to the ground radiates *x*- and *y*- oriented modes, which have the same resonant frequency. By adding shorting posts in the middle of the patch edges α (Fig. 20), the resonant frequency of the *y*-oriented mode is increased without affecting the *x*-oriented mode. This is because edges α are the radiating edges for the *y*-oriented mode. By attaching shorting posts which can be represented by inductors, the resonant frequency of the *y*-oriented mode is increased. But the *x*-oriented mode will not be affected since its

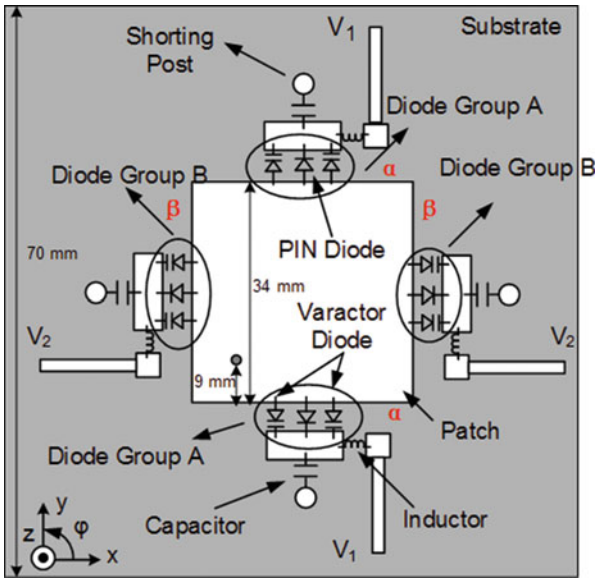

Fig. 20 Schematics of the proposed reconfigurable antenna

radiating edges are β. Similarly, by adding shorting posts in the middle of the patch edges β, the resonant frequency of the x-oriented mode is raised without affecting the y-oriented mode. Therefore, a single mode (x- or y- oriented) can be selected by shifting the resonant frequency of the undesired mode away from that of the desired one. For each mode, two varactor diodes are mounted along the corresponding radiating edges to change the resonant frequency.

Another recent design with full polarization diversity and frequency agility was presented in (Ho and Rebeiz 2014). MEMS switches are integrated into a feed network to provide four states of polarization control: vertical, horizontal, left-hand circular polarization, and right-hand circular polarization. Hyper-abrupt silicon junction tuning diodes are used to tune the antenna center frequency for each polarization. The tuning ranges are from 0.9 to 1.55 GHz and 1.1–1.5 GHz for linear and circular polarizations, respectively.

Reconfigurable Phase Shifter and Its Application in Beamforming Antennas

Phase Shifter Design Based on Reconfigurable Defected Microstrip Structure (RDMS)

Phased array antennas can achieve analogue beamforming with high gains and are extensively utilized in satellite communications, radar systems, and other military applications (Parker and Zimmermann 2002). Usually, a large number of phase

shifters are employed in a phased array antenna, and thus their cost, size, and integration method are of great concerns (Hansen 1998). The most popular phase shifters used in phased array antennas are diode ones (White 1974; Davis 1975) and ferrite phase shifters (Whicker 1973). Diode phase shifters have fast switching time, a low weight, a low cost but a high insertion loss, whereas ferrite phase shifters are relatively bulky and heavy, and require significant switching power compared with diode ones.

Recently, phase shifters based on defected ground structure (DGS) are developed (Patil et al. 2012; Han et al. 2005; Shafai et al. 2004). For most of the designs, multi-layer structures and micro electromechanical systems (MEMS) are used. Therefore, they suffer from a high cost and high fabrication complexity, and they are difficult to be integrated into microstrip systems, which substantially limits their applications. As a dual structure of DGS, the defected microstrip structure (DMS) also has the potential to provide a phase shift. In (Ye et al. 2012), C-shaped slots are etched on microstrip lines in the feed network for phase alignment. However, each slot only has a fixed phase delay of 3^0 at 12.5 GHz. In order to have controllable phase shift, Can et al. proposed compact phase shifters using reconfigurable defected microstrip structure (RDMS) for phased array antennas (Ding et al. 2014; Ding et al. 2015).

Figure 21 shows the structure of the RDMS unit based on a 50-Ω microstrip line for the phase shifter design. As depicted in the figure, a rectangular slot with a size of $W_{slot} \times L_{slot}$ is etched on the microstrip line to introduce a defect. PIN diodes are inserted into the edges of the slot area, which enables structural reconfiguration and results in a RDMS unit. Capacitors and metal stubs used for capacitor mounting are placed in the middle of the slot to achieve RF continuity as well as to provide DC isolation. The RDMS unit has two working states, the "All-on" and "All-off" states, when the diodes are turned "on" and "off," respectively. In the All-on state, both the diodes and capacitors allow the currents to go through them with minor losses. Numerical simulations find that the RDMS unit behaves like a uniform microstrip line in this state. In the All-off state, the currents across the diodes are blocked, resulting in a different current distribution as shown in Fig. 21b. It is noted that in the All-off state, the current path is longer than that in the All-on state, which produces a phase shift. The phase shift value is in proportional to the difference of the electrical length of the current path in the two states, which is affected by W_{slot} and L_{slot}. An RDMS unit with $\{W_{slot}, L_{slot}\} = \{2\text{ mm}, 3.3\text{ mm}\}$ was fabricated as an example. Figure 22a, b, and c shows the picture of the fabricated RDMS unit, the measured insertion losses, and phase shifts, respectively. According to the measured results, the fabricated RDMS unit produces a phase shift of 20^0 with an insertion loss of 1.1 dB at 5.2 GHz.

Larger phase shift values can be achieved by cascading several RDMS units described above. A 2-RDMS phase shifter cascading two RDMS units is shown in Fig. 23a, which can realize a 40^0 phase shift. Furthermore, a phase shifter cascading four RDMS units is shown in Fig. 23b. By using two biasing voltages, phase shifts of 44° and 88° can be obtained at 5.2 GHz.

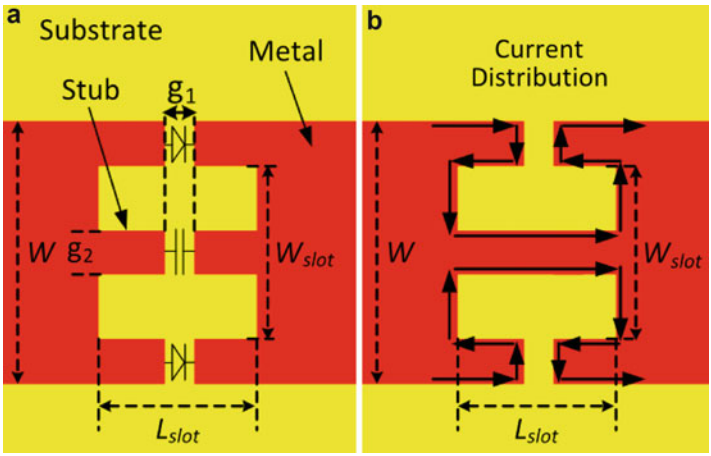

Fig. 21 (**a**) Structure of the RDMS unit. (**b**) All-off state current distribution

Application in a 4-Element Phased Array

The above described phase shifters have been employed in a 4-element phased array feed network as shown in Fig. 24. The array is designed to be able to switch its main radiation beam to 0^0, -15^0 and 15^0 in the H plane. In this design, 3 Wilkinson power dividers are employed to split the power while 8 phase shifters are integrated in the feed network to realize 50° progressive phase differences between the array elements at 5.2 GHz. Each phase shifter is composed of two RDMS units with $W_{slot} = 2\ mm$ and $L_{slot} = 3.6\ mm$. For the first-level power divider, there are 2 phase shifters at each of the 2 branches. For the second-level, there is 1 phase shifter at each of the 4 branches. Two bias DC voltages labelled by *V1* and *V2* are employed to control the phase shifters. There are 4 different working states of the phased array. When voltages *V1* and *V2* are "+,+," "–,–," "+,–," and "–,+," the phased array can work in the "All-on," "All-off," "left-on-right-off," and "Left-off-right-on" states. In the All-on and All-off states, the array elements are in phase so that the beam is not tilted. In the left-on-right-off and Left-off-right-on states, phase advances and delays of 50^0 between the array elements are obtained, respectively. Therefore, beam tilts of -15^0 and 15^0 are realized. The measured far-field pattern of the array is given in Fig. 25.

Reconfigurable Leaky Wave Antennas

Introduction

Leaky wave antennas can be regarded as transmission lines that gradually leak the energy out into free space. The direction in which the energy is radiated from a leaky wave antenna, θ, is determined by the phase constant β, of the leaky wave

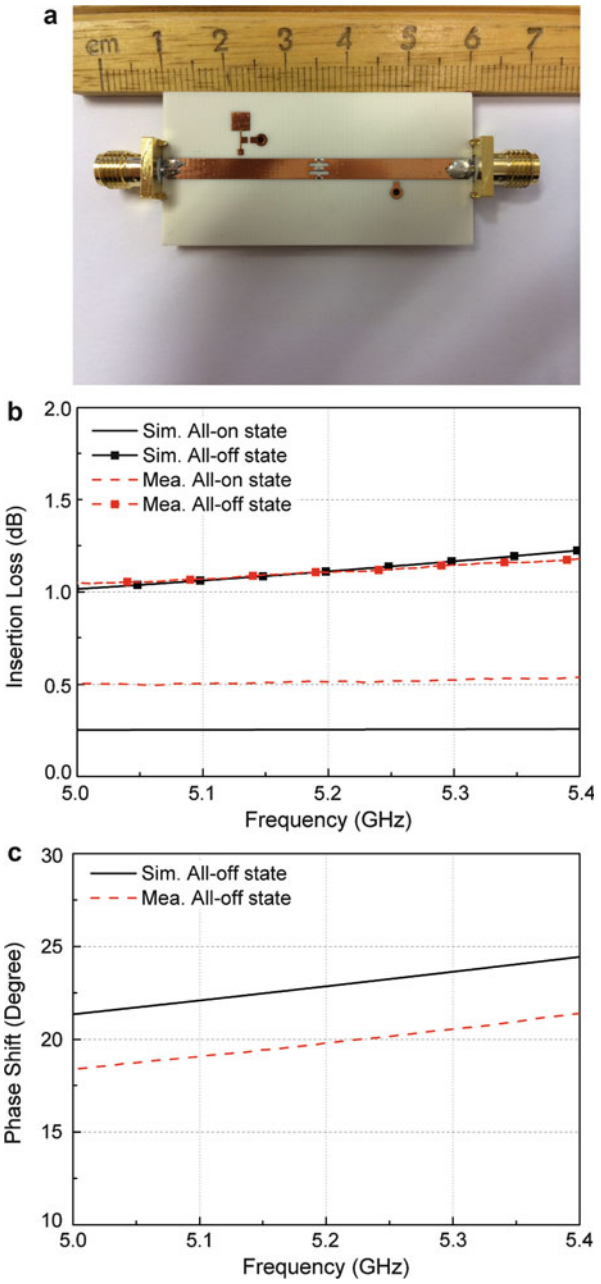

Fig. 22 (**a**) Photo of the fabricated 1-bit phase shifter. The simulated and measured results of the (**b**) insertion losses and (**c**) phase shift

along the transmission line (Goldstone and Oliner 1959), as shown in Fig. 26. The beamwidth of a leaky wave antenna is determined by the length of the leaky aperture, which must be illuminated by proper control over the leakage rate α (Goldstone and Oliner 1959).

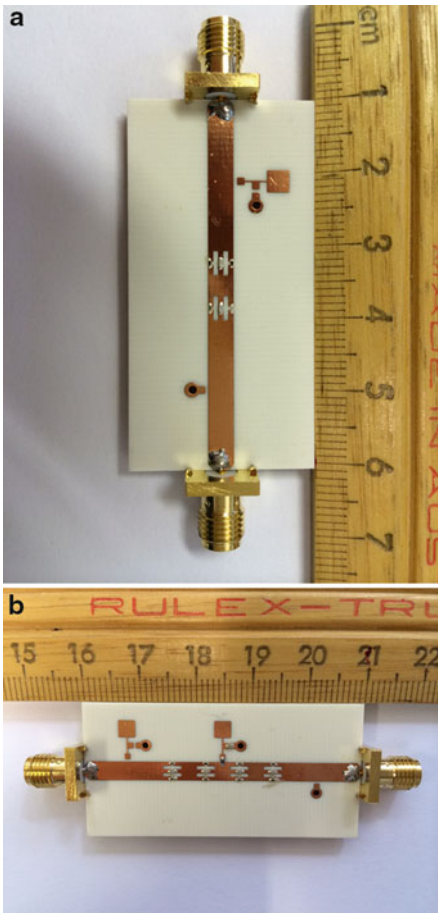

Fig. 23 (**a**) 2-RDMS phase shifter; (**b**) 4-RDMS phase shifter

The concept of leaky-wave antennas has been around for decades (Horn et al. 1980). Compared with reflector and lens antennas, it has the advantage that no protruding feed is needed so the antenna can have a very low profile. Compared with array antennas, it does not need a feed network which can become very lossy for large arrays. The phase constant of a leaky wave antenna is typically a function of the operating frequency, and this fact can be used to steer the beam direction by sweeping the operating frequency.

In the last decade, the fastest growth of the wireless communications industry and a multitude of wireless communications system standards have been witnessed. Wireless communication systems normally operate in a given frequency band defined by the spectrum regulators. Therefore, the inherent frequency scanning nature of leaky wave antennas has very limited use. To this end, there is a great need to develop pattern reconfigurable (beam-steering) leaky wave antennas which can be used to exploit the complexity of the propagation channel. Furthermore, leaky wave antennas have relatively narrow bandwidth, typically of only a few percent.

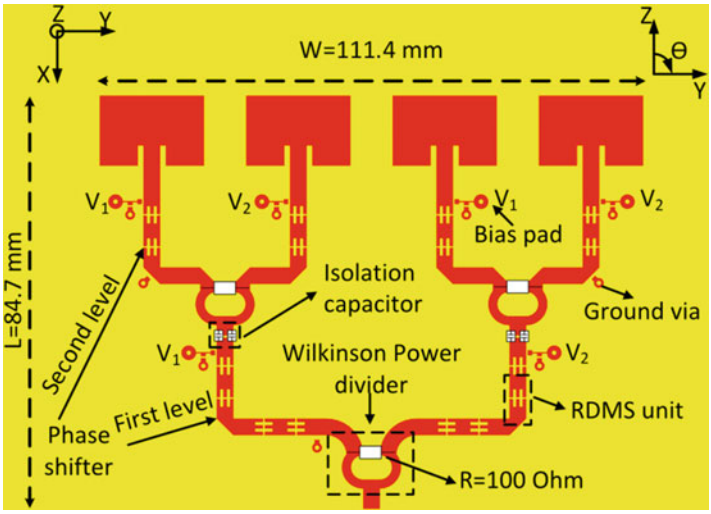

Fig. 24 The 4-element phased array prototype

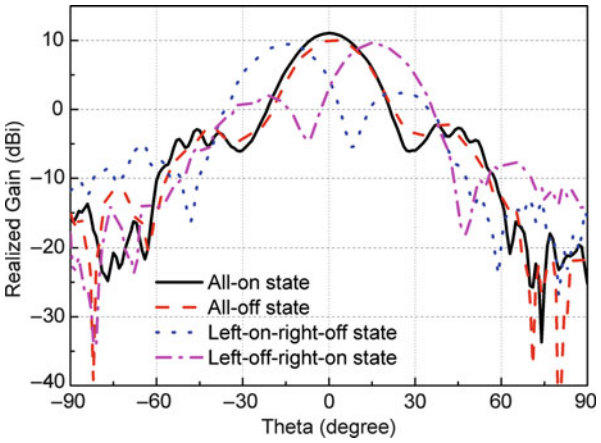

Fig. 25 The measured far-field pattern of the phased array

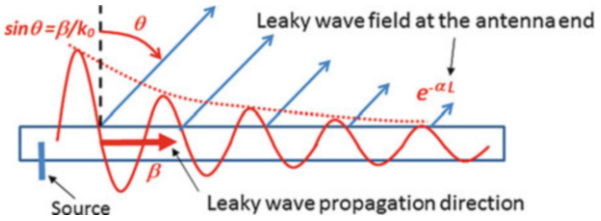

Fig. 26 Scheme of a leaky wave antenna

However, given that wireless communications systems do not need a simultaneous wide bandwidth, a frequency reconfigurable (tunable) leaky wave antenna would serve as a good candidate for many applications.

The frequency-dependent nature of leaky wave antennas has limited their applications in modern communication systems, which generally require fixed frequency operation for effective channelization. In the past, significant efforts have been directed toward developing frequency-independent leaky wave antennas. Horn et al. (Horn et al. 1980) used PIN diodes as switches and electrically changed the radiation angle by controlling the guided wavelength. In their approach, however, only two discrete radiation angles were present because diodes have only two states, namely biased and unbiased. Maheri et al. (Maheri et al. 1988) reported a magnetically scannable leaky-wave antenna built on a ferrite slab structure, in which the radiation angle is scanned by tuning the DC magnetic field. In (Huang et al. 2000), Huang et al. applied PIN diodes as switches to control the period of the structure, and the reconfigurability was limited to two discrete radiation angles.

In (Sievenpiper 2005), Sievenpiper employed a high impedance surface which called a textured surface to develop a leaky wave antenna which can scan from backward to forward directions from -50^0 to 50^0. In the design, varactor diodes incorporated into the structure allow electronic control of the reflection phase and the surface wave properties. This tunable textured surface is then used as an electronically steerable leaky wave antenna by coupling energy into a leaky wave band using a flared notch antenna. The textured surface consists of a periodic lattice of small mushroom-shaped protrusions made of square metal plates, connected to a common ground plane by vertical metal pins. These pins are alternatively connected to and protruded through the ground-plane to allow the controlling voltage to be applied. The square plates are all connected to each other with varactor diodes. By exploiting multiple degrees of freedom which the surface geometry provided, the author achieved independent control of the magnitude and phase of the surface wave radiation, so the antenna can be programmed to have a large effective aperture over the entire scan range.

Left-handed (LH) materials characterised by simultaneously negative permittivity and permeability were introduced theoretically by Veselago (Veselago 1968) and investigated experimentally by Shelby et al. (Shelby et al. 2001). The propagation constant of a left-handed material is negative, representing a phase advance, whereas that of a right handed material is positive, representing a phase lag. Combining structures with LH and RH contributions results in a composite RH-LH (CRLH) structure, which can be used to realize both forward and backward scanning. This concept was first introduced using a transmission line structure in (Liu et al. 2002). In (Lim et al. 2005), a metamaterial-based electronically controlled transmission line structure incorporating varactor diodes was proposed as a leaky-wave antenna with tunable radiation angle and beamwidth functionalities. This structure is, in essence, a CRLH microstrip structure incorporating varactor diodes for fixed-frequency voltage-controlled operation. Angle scanning at a fixed frequency is achieved by modulating the capacitances of the structure by adjusting a uniform bias voltage applied to the varactors. Beamwidth tuning is obtained by making the structure

non-uniform by the application of a non-uniform bias voltage distribution of the varactors. A 30-cell leaky wave antenna structure, incorporating both series and shunt varactors for optimal impedance matching and maximal tuning range, was designed. This prototype exhibits continuous scanning capability from $+50^0$ to -49^0 by tuning the bias voltages from 0 to 21 V at 3.33 GHz. A maximum gain of 18 dBi at broadside is achieved, but the gain variation with scan angle is large. In addition, it provides half-power beamwidth variation of up to 200 % with comparison to the case of uniform biasing.

Employing tunable partially reflective surfaces and high impedance surfaces in Fabry-Pérot structures proved to be another way of achieving frequency reconfigurability and pattern reconfigurability in leaky wave antennas effectively. The authors of this chapter have conducted a systematic study in this regard in recent years which will be presented in the following sections.

Frequency Reconfigurable Fabry Pérot Antenna

Fabry-Pérot leaky wave antennas have the advantages of low profile, simple construction and high directivity. They are created by placing a partially reflective surface (PRS) around half a wavelength above a ground plane containing a low directivity source antenna (Trentini 1956; Feresidis and Vardaxoglou 2001; Feresidis et al. 2005; Wang et al. 2006; Weily et al. 2008). The PRS is usually a periodic array of dipoles, patches or slots on a dielectric substrate. If the ground plane is replaced with a high impedance surface (HIS), the profile of the antenna can be significantly reduced (Feresidis et al. 2005; Wang et al. 2006). A significant drawback of the Fabry-Pérot leaky wave antenna is the narrow operating bandwidth, due to the high Q factor of the Fabry Pérot cavity. However, the utility can be improved by making the operating frequency reconfigurable, through the use of a tunable HIS on the lower surface of the cavity where each cell of the HIS is tuned through the voltage applied to a pair of varactor diodes (Hum et al. 2005; Hum et al. 2007).

The geometry of the Fabry-Pérot leaky wave antenna, comprising a PRS, tunable HIS and stacked patch feed antenna, is shown in Fig. 27 (Weily et al. 2008). Its operating frequency was designed to be tuned from 5.2 to 5.775 GHz to enable use in WLAN applications. Referring to Fig. 28, the cavity height Lr can be expressed in terms of the operating wavelength λ_0, and the reflection phase of the PRS φ_1 and tunable HIS φ_2 as follows (Wang et al. 2006).

$$L_r = \left(\frac{\varphi_1 + \varphi_2}{\pi}\right)\frac{\lambda_0}{4} + \frac{\lambda_0}{2} \tag{1}$$

Since φ_2 is a function of the varactor tuning voltage, it is possible to reconfigure the operating frequency of the antenna. Increasing the tuning voltage gives an increase in the antenna resonant frequency, while lowering the voltage reduces the resonant frequency. In this implementation the PRS is made from 18 mm × 18 mm square metallic patches placed on a 0.8 mm thick FR4 substrate ($\varepsilon_r = 4.4$, $tan\delta = 0.018$),

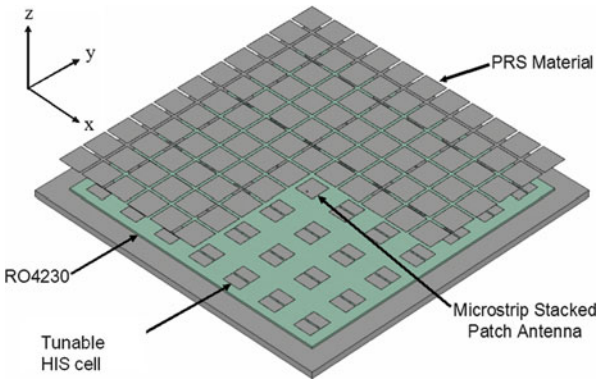

Fig. 27 Geometry of the frequency reconfigurable FP LWA

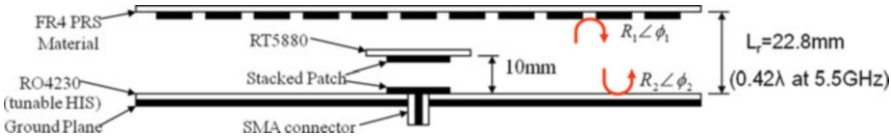

Fig. 28 Schematic of the frequency reconfigurable FP LWA showing reflection coefficients of the PRS and HIS

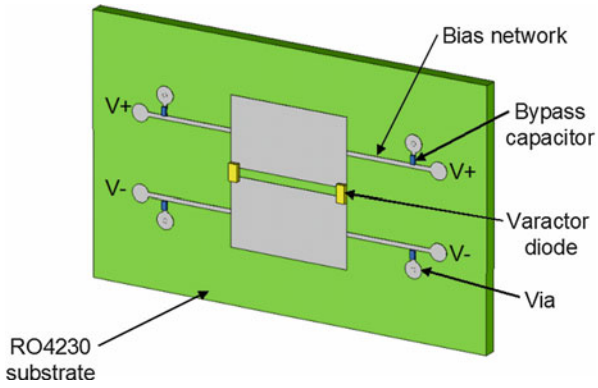

Fig. 29 Geometry of the tunable HIS unit cell

with a periodicity of 20 mm in both *x*- and *y*-directions. A total of 48 tunable HIS cells are used on a 1.524 mm thick Rogers RO4230 substrate ($\varepsilon_r = 3.0$, $tan\delta = 0.0023$). Patch dimensions are 14 mm by 17 mm, with a 1 mm air gap between its two halves for placement of the varactor diode pair. Both substrates have lateral dimensions of 240 mm by 240 mm. A stacked probe-fed patch was chosen for the source because simulations showed it gave better matching as the HIS surface was tuned, compared to a single patch.

Figure 29 depicts the geometry of the tunable HIS cell used in the antenna, and includes the bias network which consists of 0.5 mm wide high impedance lines, 2.2 pF

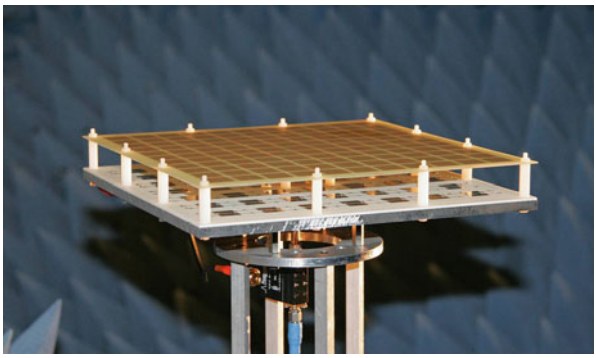

Fig. 30 Photograph of the frequency reconfigurable FP LWA prototype

bypass capacitors and vias. The tunable HIS cell is based on a design from (Hum et al. 2005), used in a reconfigurable reflectarray (Hum et al. 2007). However, it has been modified to include a distributed element bias network to allow simultaneous biasing of a complete row of tunable HIS cells. A photograph of the fabricated prototype antenna is shown in Fig. 30. Various nylon spacers have been used to position the PRS above the tunable HIS, and the coupled patch above the driven patch. A low-loss bias tee, which may be observed behind the antenna, is used to provide the bias voltage to the tunable HIS cells, and thus reconfigure the antenna's operating frequency. The varactor diodes used in the prototype were also "matched" by the manufacturer to ensure variations between the devices were as small as possible. The measured directivity versus frequency is plotted in Fig. 31 for six different bias voltages, which correspond to six different junction capacitances of the varactor diode. It is clear from Fig. 31 that the measured operating frequency tunes from 5.2 to 5.95 GHz. The measured reflection coefficient of the antenna is shown in Fig. 32 and tracks the directivity peaks of Fig. 31 for the corresponding six bias voltages.

Pattern Reconfigurable Leaky Wave Antennas

As mentioned earlier, one of the disadvantages of leaky wave antennas is that the radiation beam typically scans with the operating frequency. This is often problematic as, for many applications, it is required to have a fixed frequency band when the antenna beam is scanned. With one dimensional leaky wave antennas, this can be done by electronically reconfiguring the leaky-line boundary condition. Using active devices such as varactor diodes or MEMS, the leaky-mode complex propagation constant can be altered, thus producing the desired control of the scanning beam. Using the Fabry-Pérot structure, a number of techniques have been developed to scan the beam of a leaky-wave antenna at a fixed frequency.

Half-space scanning 1D Fabry-Pérot leaky wave antenna

As the first step, a one-dimensional half-space scanning leaky wave antenna is designed, as shown in Fig. 33a. This structure is inspired by the passive 1D

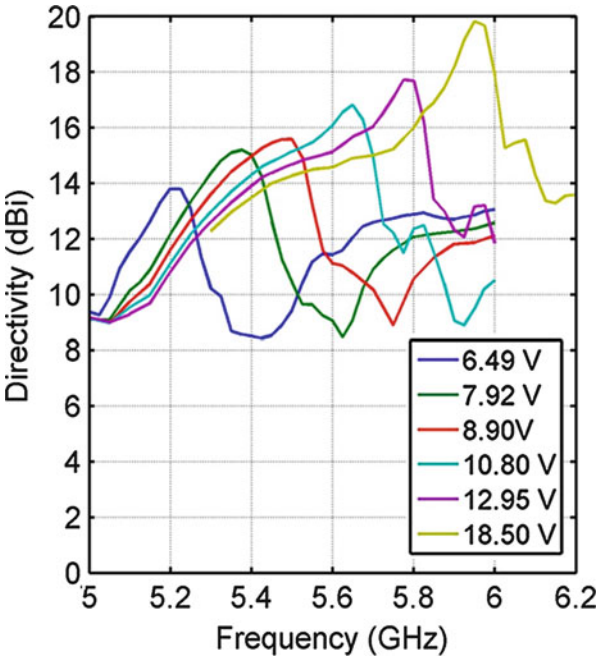

Fig. 31 Measured directivity of the frequency reconfigurable FP LWA for six different bias voltages

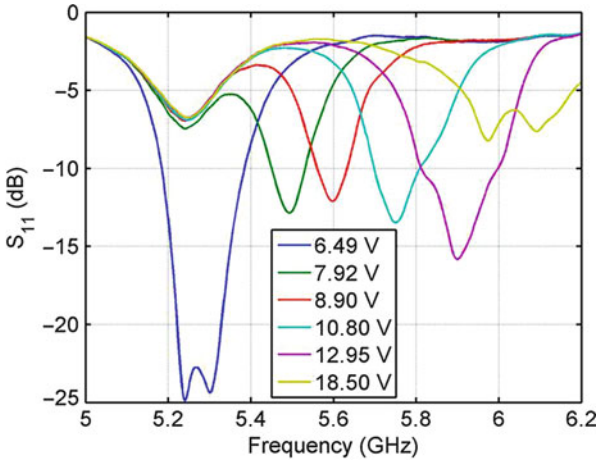

Fig. 32 Measured reflection coefficient of the frequency reconfigurable FP LWA for six different bias voltages

Fabry-Pérot leaky wave antenna presented in (García-Vigueras et al. 2011), where a Fabry-Pérot cavity made of a top partially reflective surface (PRS) and a bottom high impedance surface (HIS) enables control of the leakage rate (α) and the phase constant (β) of the leaky mode through design of the physical length of the resonant patches. In this case, the structure provides electronic scanning of the main beam in the forward quadrant, at a fixed operating frequency (Guzmán-Quirós et al. 2012a), by replacing the passive HIS of (García-Vigueras

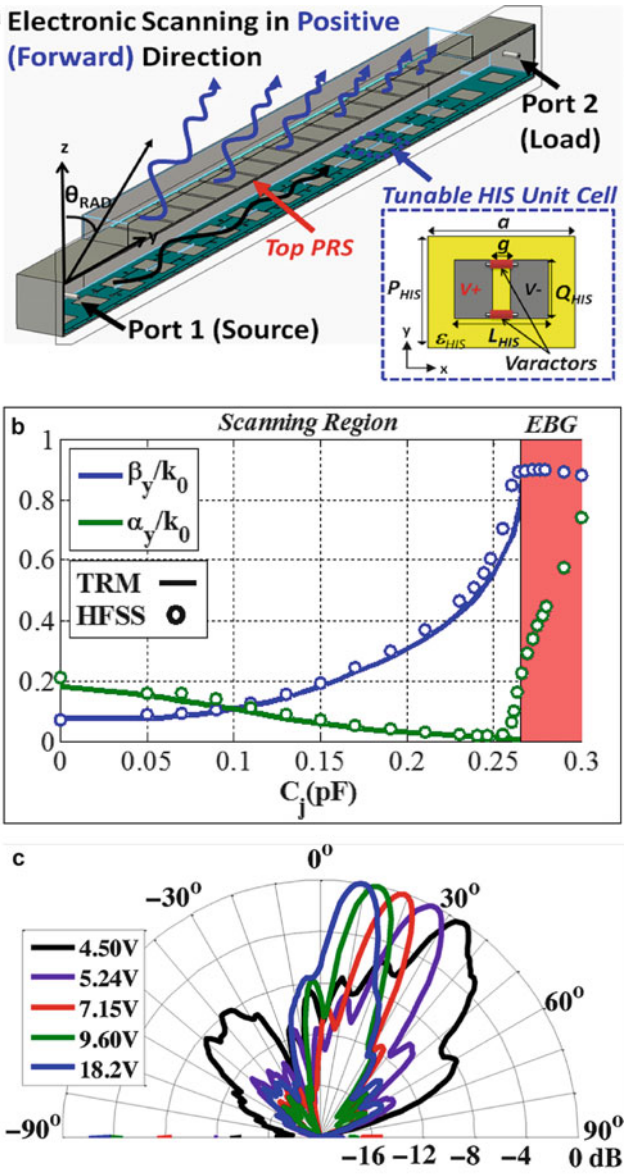

Fig. 33 (**a**) Scheme of a half-space scanning 1D FP LWA (**b**) Dispersion curves versus Cj and (**c**) Measured radiation patterns (H-plane) for different V_R at 5.5 GHz

et al. 2011) by a bottom tunable high impedance surface (HIS) loaded with varactor diodes (Guzmán-Quirós et al. 2012a). Now, the β of the leaky wave antenna can be controlled electronically as a function of the tunable junction capacitance (C_j) introduced by the varactor diodes which load the HIS patches

(Fig. 33a) (Weily et al. 2008; Hum et al. 2005; Hum et al. 2007). This C_j is tuned by the DC bias voltage (V_R) applied to the diodes.

The control of the LM dispersion with C_j is demonstrated in Fig. 33b, showing the normalized phase (β/k_0) and leakage (α/k_0) rates as a function of C_j for a fixed operating frequency of 5.5 GHz, where k_0 is the free-space wave number in air. It is shown how the LM phase constant increases with C_j in the scanning region defined in the range $C_j = [0\text{ pF},0.27\text{ pF}]$. As β/k_0 is related with the main beam radiation angle θ_{RAD} by $sin(\theta_{RAD}) \approx \beta/k_0$ (Goldstone and Oliner 1959), a half-space electronic scanning of the fan beam direction with V_R is obtained in the positive quadrant from $\theta_{RAD} = +9°$ to $\theta_{RAD} = +34°$, as experimentally confirmed by the measured radiation patterns shown in Fig. 33c.

Full-space scanning 1D Fabry-Pérot leaky wave antennas

The structure of a symmetrically-fed 1D Fabry-Pérot leaky wave antenna is depicted in Fig. 34a. This antenna is conceived to extend the half-space scanning range obtained from the previous 1D Fabry-Pérot leaky wave antenna design, to a full-space scanning range. This is achieved by taking advantage of the electromagnetic band-gap (EBG) property that is presented in the Fabry-Pérot cavity for low values of the tuning voltage V_R (Guzmán-Quirós et al. 2012b). As shown in Fig. 34b, an EBG zone extends beyond the scanning region for $C_j = [0.27\text{ pF}, 0.3\text{ pF}]$. LM propagation along the FP waveguide is prevented in this zone. A central coaxial probe feed divides the original antenna in to two symmetric leaky lines: LWA_{LEFT} and $\text{LWA}_{\text{RIGHT}}$. Each one is separately biased by V_L or V_R. Therefore, two leaky waves which are oppositely launched by the central coaxial feed yield two radiation patterns whose main beam pointing angles can be independently controlled based on the dispersion properties of the 1D Fabry-Pérot leaky wave antenna (Guzmán-Quirós et al. 2012a).

Using the scanning and EBG properties of the HIS-loaded Fabry-Pérot cavity, the leaky wave antenna can be electronically tuned to propagate/radiate energy or to serve as a reflector, depending on the electronic tuning of the HIS. Hence, the symmetrically-fed 1D Fabry-Pérot leaky wave antenna can be electronically tuned to operate in three different regimes:

(1) Backward scanning regime ($\theta_{RAD} < 0°$): LWA_{LEFT} must be tuned inside the scanning region ($C_{jL} < 0.27$ pF) while $\text{LWA}_{\text{RIGHT}}$ is fixed at EBG region ($C_{jR} = 0.3$ pF). In this way the input signal is guided to the left side of the LWA (no energy travels to the right side), providing scan at negative angles.
(2) Forward scanning regime ($\theta_{RAD} > 0°$): This is the symmetrical case. LWA_{LEFT} is operated in the EBG region ($C_{jL} = 0.3$ pF) and $\text{LWA}_{\text{RIGHT}}$ is tuned in the scanning region to provide beam steering at positive angles (with $C_{jR} < 0.27$ pF).
(3) Broadside radiation ($\theta_{RAD} = 0°$): Radiation at boresight can be obtained by launching two oppositely-directed leaky waves. To this end, LWA_{LEFT} and $\text{LWA}_{\text{RIGHT}}$ are tuned at the same operating point inside the scanning region at or below the splitting condition $\beta = \alpha$ (Lovat et al. 2006) (which is obtained for $C_{jR} = C_{jL} = 0.1$ pF in this case), so that the fields on the two sides of the antenna merge to form a single beam radiating at $\theta_{RAD} = 0°$.

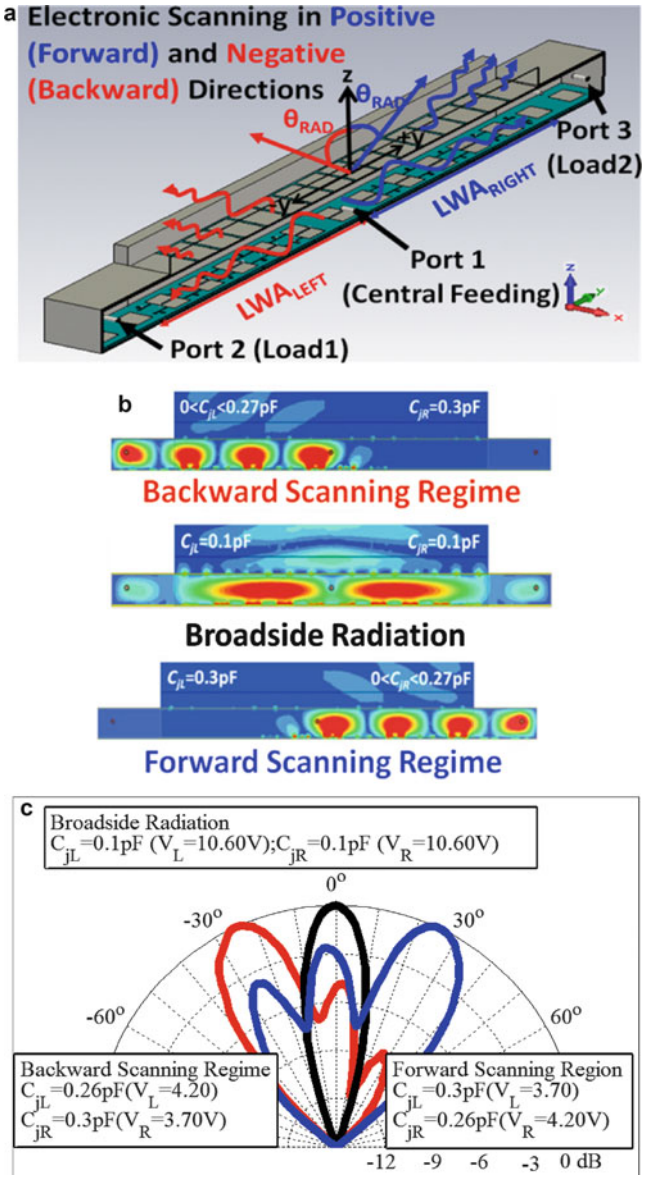

Fig. 34 (**a**) Scheme of full-space scanning 1D FP LWA (**b**) Electric field distribution along the 1D FP LWA structure and (**c**) Measured normalized radiation patterns (H-plane) at different operating regions (5.5 GHz)

For a better physical insight, the electric field distribution inside the Fabry-Pérot cavity is depicted in Fig. 34b for the three operating configurations, showing how the input energy can be routed to the right or left directions depending on the tuning voltage of the varactor diodes. Finally, measured radiation patterns of a fabricated

prototype are shown in Fig. 34c, confirming full-space electronic scanning from −25° to +25° at 5.5 GHz.

Full-Space scanning 2D Fabry-Pérot leaky wave antennas

The EBG routing and scanning concepts described earlier can be extended from 1D to 2D Fabry-Pérot leaky wave antennas, so that 2D electronic scanning (azimuth and elevation) is obtained without using phased-arrays (Debogovic and Perruisseau-Carrier 2014). As a proof of the concept, a 2D Fabry-Pérot antenna was designed using a 2D PRS at the top and 2D tunable HIS at the bottom. The varactors have been arranged into four independently biased azimuthal sectors (SA to SD, as shown in the scheme of Fig. 35a). In this case, a cylindrical LM is excited at the centre of the 2D Fabry-Pérot cavity by a horizontal dipole oriented along the x axis (Fig. 35a). This cylindrical LM is thus TM-polarized in sectors SA and SC (x-axis), TE-polarized in sectors SB and SD (y-axis), and a hybrid TE/TM LM for other directions (Ip and Jackson 1990). As in the 1D case, the LM will be routed towards a given sector by tuning it into the scanning region while the rest of the sectors are tuned to the EBG region.

Therefore, pencil beams which are scanned in the elevation plane (θ_{RAD}) can be created for discrete azimuthal (ϕ_{RAD}) angles defined by the four sectors. As a result, four radiation regions can be defined according to the direction of propagation of the wave:

(1) Radiation by TM LM propagating along the $\pm x$ axis. SA or SC is active (tuned at the scanning region) while all other sectors are inactive (tuned at EBG region).
(2) Radiation by TE LM propagating along the $\pm y$ axis. SB or SD is active and all other sectors are inactive.
(3) Radiation by hybrid TE/TM LM propagating along the oblique directions when two adjacent sectors are active (configurations SA&SB, SB&SC, SC&SD or SD&SA) and the other two are tuned to the EBG region.
(4) Broadside radiation. Optimal directive pencil beam radiating at boresight can be obtained when all the sectors are active and tuned at or below the splitting condition (Lovat et al. 2006).

Four different configurations of the sectors are illustrated in Fig. 35b, c), showing the simulated near fields inside the 2D Fabry-Pérot cavity and their respective radiation patterns. From the guided fields depicted in Fig. 35b, it is observed how the antenna aperture illumination can be modified by changing the activation of the azimuthal sectors. These illuminations lead to the synthesis of radiated pencil beams which can be steered to discrete azimuthal angles $\phi_{RAD} = [0°, 45°, 90°, 135°, 180°, 225°, 270°, 315°]$. This is demonstrated by the position of the pencil beam in the radiation patterns obtained in Fig. 35c for each sector configuration. Moreover, for any constant azimuthal angle ϕ_{RAD}, tuning of the elevation scanning angle in the range $\theta_{RAD} = [5°, 25°]$ can be obtained, by properly tuning the active sector inside the scanning range. Finally, the broadside case is also obtained when the four sectors are tuned to (or below) the splitting

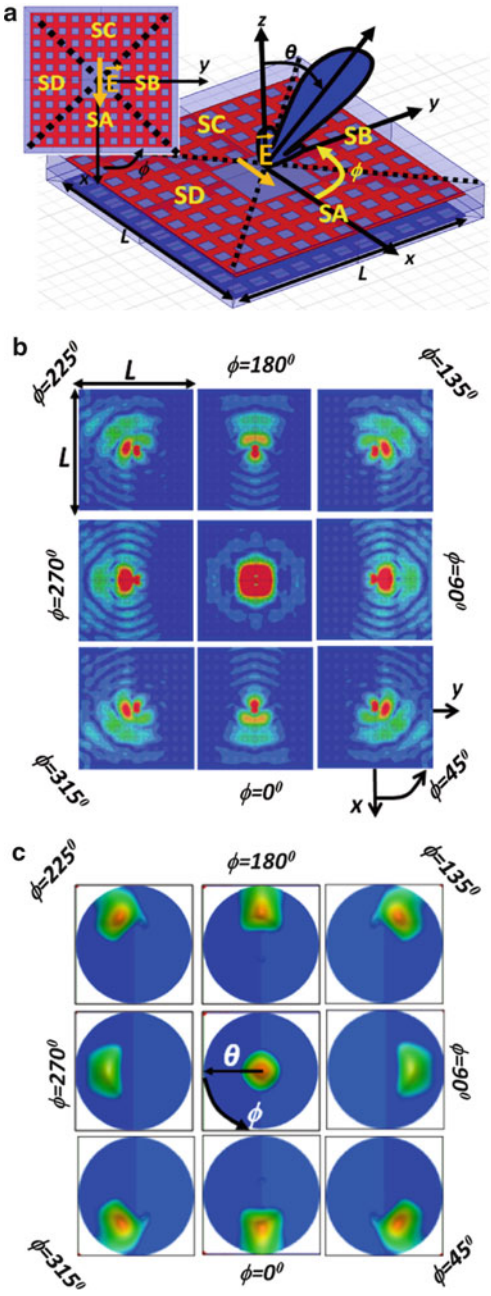

Fig. 35 Extension of the EBG routing mechanism for full-space electronic scanning in 2D FP LWAs: (**a**) HFSS 3D model of the tunable 2D FP ($A = 5.4\lambda_0 \times 5.4\lambda_0$), (**b**) Near fields inside the 2D FP cavity for several configurations of the sectors and (**c**) Radiation pattern in U-V coordinates (θ range represented [0°,45°])

condition, resulting in a cylindrical LM covering all sectors (Fig. 35b) and a pencil beam pointing at boresight (Fig. 35c).

From these results, it is demonstrated that continuous elevation scanning and discrete azimuthal sectorization can be electronically obtained. This requires accurate control of the dispersion properties of TE, TM and hybrid TE/TM cylindrical LMs.

Reconfigurable 1D SIW LWA

Reconfigurable LWAs can also be realized in substrate integrated waveguide (SIW), taking advantage of the planar, low cost, low loss, easy integration with planar circuits, and simple excitation properties of this technology (Xu and Wu 2005). Several reconfigurable LWAs have been proposed in the last decade using metamaterial CRLH microstrip leaky lines (Liu et al. 2002; Lim et al. 2005) in order to obtain electronic beam steering (Liu et al. 2002) or even beamshaping (Lim et al. 2005). In this section, two structures are presented to operate at ISM frequency band (5.5 GHz). The first one is a reconfigurable 1D antenna in SIW technology (1D SIW LWA), which is based on the non-reconfigurable static design presented in (Martínez-Ros et al. 2012a). This design is modified to provide full reconfiguration of its radiation pattern (radiation angle and beamwidth) using two control lines. It must be highlighted that it is the first time that it is demonstrated simultaneous electronic reconfiguration over the scanning angle and the beamwidth, without using complicated metamaterial unit-cells (Lim et al. 2005). The second structure is a radial array of SIW LWAs as originally proposed in (Martínez-Ros et al. 2012b). The introduction of electronic reconfiguration in the 2D LWA provides electronic elevation scanning and azimuth sectorization (as in the 2D FP LWA studied in the previous section), as well as electronic shaping of the pencil beam.

A schematic of the proposed full-reconfigurable 1D SIW LWA is presented in Fig. 36. The antenna consists of a double-layer structure with a ground plane in between. The top layer holds the SIW, which is loaded with a tunable PRS and a tunable HIS in substrate integrated technology. Both PRS and HIS are SIW versions of the Fabry-Pérot sheets. They are made of arrays of metallic posts periodically arranged at a certain distance (called PRS posts and HIS posts in Fig. 36). The PEC plane needed for the HIS is made of a dense arrangement of via-holes at a certain distance D from the HIS posts. Each post is connected by a through via to a varactor diode loaded in a microstrip stub, which is etched to the second layer (the control layer). Teflon substrates with $\varepsilon_r = 2.2$ and thicknesses $h_1 = 3.17$ mm and $h_2 = 0.127$ mm are used for the radiation and control layers, respectively.

The PRS and HIS are separated by a distance W, comprising a resonant cavity that is analogous to the FP air-filled cavities of the antennas presented in the previous section, but in a substrate integrated technology. It is interesting to note that the radiation mechanism of this 1D SIW LWA is quite similar to the previous 1D FP LWA; according to the defined coordinate system, the FP antennas resonate between the PRS-HIS cavity, so the resonance is produced along the z-axis, whereas in the 1D SIW LWA case, this resonance arises along the x-axis. Moreover, in this case the PRS is also a tunable structure, so that it allows electronic control of the leakage rate

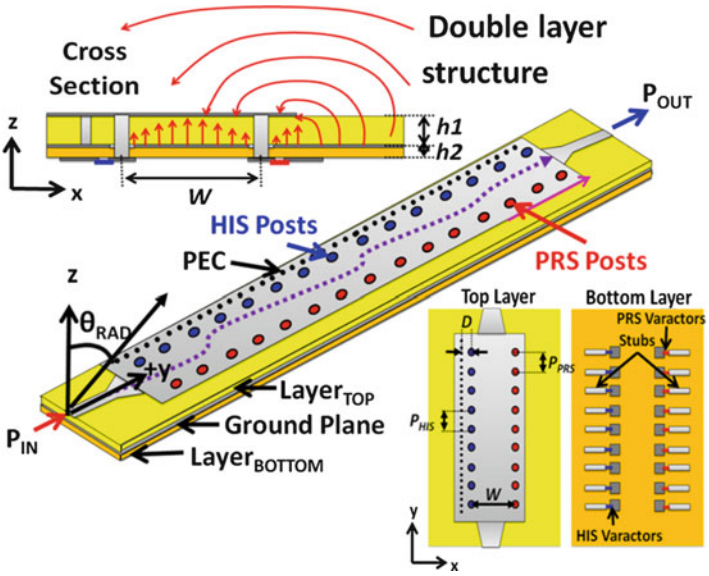

Fig. 36 Schematic of full-reconfigurable 1D SIW LWA: 3D model, cross section and front and rear views of the structure

(α) of the LM which is related to the half-power beamwidth and directivity (Goldstone and Oliner 1959). On the other hand, the tunable HIS controls the scanning angle by altering the LM phase constant (β), as described for the previous FP antennas. Both SIW PRS and HIS are independently biased, to enable independent and simultaneous electronic control of the radiation angle and beamwidth of the scanned fan beam.

A 1D SIW LWA has been simulated at a fixed frequency of 5.5 GHz in order to demonstrate the concept. The antenna length is $L_A = 3\lambda_0$, and it is terminated with a short-circuit load in order to estimate the variations in the leakage rate from the reflected lobe. The tuning parameters which reconfigure the antenna are the varactors' junction capacitances introduced at the HIS and the PRS circuits, C_{jHIS} and C_{jPRS}, respectively. Simulated radiation patterns at 5.5 GHz for six different configurations are presented in Fig. 37. The values of the scanning angle (θ_{RAD}), the normalized attenuation constants (α/k_0), and associated -3 dB beamwidth ($\Delta\theta$), are listed in Table 1 for each case. It is demonstrated that the scanning angle and the beamwidth can be simultaneously controlled by properly adjusting the two independently tunable parameters, namely C_{jHIS} and C_{jPRS}. Particularly, cases 1 and 2 show a beam scanned at $\theta_{RAD} \approx 15^\circ$ with variable beamwidths $\Delta\theta = 11^\circ$ and $\Delta\theta = 36^\circ$, as it can be seen in the radiation patterns of Fig. 37a. The synthesis of narrow and broad beams is repeated for other scanning angles, namely $\theta_{RAD} \approx 24^\circ$ and $\theta_{RAD} \approx 34^\circ$, for cases 3–4 and 5–6, respectively. The normalized leakage rate is estimated for each

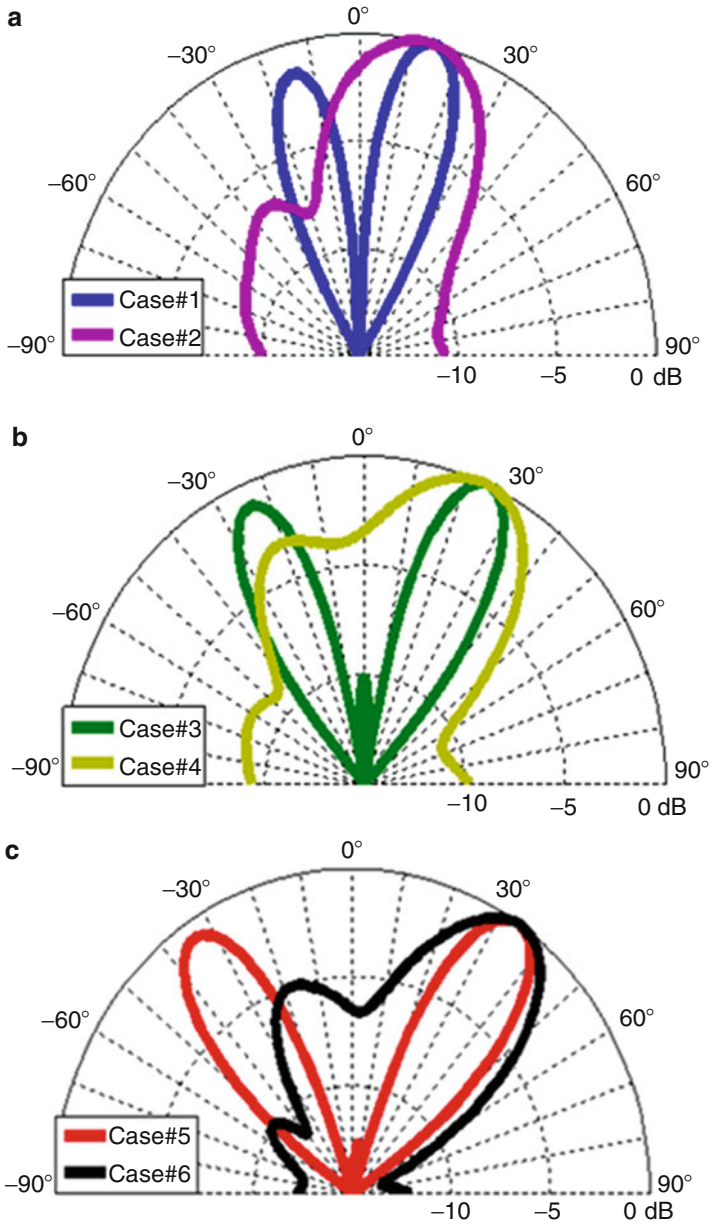

Fig. 37 Simulated radiation patterns (normalized directivity in dB) for different Cj_{HIS} & Cj_{PRS} configurations (5.5 GHz): (**a**) Cases 1 and 2, (**b**) Cases 3 and 4, and (**c**) Cases 5 and 6

Table 1 Results for different combinations of C_{jHIS} and C_{jPRS}

Case#	C_{jHIS}(pF)	C_{jPRS}(pF)	θ_{RAD}(deg)	α/k_0	$\Delta\theta$(deg)
1	0.45	0.2	15°	0.0036	11°
2	0.2	0.6	13°	0.0360	36°
3	0.5	0.2	24°	0.0017	13°
4	0.23	0.6	24°	0.0120	39°
5	0.6	0.2	34°	0.0009	16°
6	0.25	0.6	35°	0.0070	30°

case, by measuring the level between the main lobe and the mirrored reflected lobe (Goldstone and Oliner 1959). As expected, narrow beams correspond to low leakage rates, while broader beams arise from increased leakage rate. A one-order-of-magnitude variation in α/k_0 is obtained for all scanning angles. To conclude, these preliminary simulations verify that the proposed tunable 1D SIW LWA allows flexible electronic tuning of the scanning angle and the directivity at a fixed frequency of 5.5 GHz. Future work will provide a more detailed study of the dispersion curves of the antenna with C_{jPRS} and C_{jHIS}, and the optimal design and fabrication of a full prototype.

Summary

In the last decade, substantial achievements on reconfigurable antennas (RAs) have been made and several inherent challenges have been successfully overcome, including the design of dual-band polarization RAs and high-gain beam-steering pattern RAs. Furthermore, the authors of this chapter have employed novel reconfiguration techniques to achieve low-cost, low-loss phase shifters and reconfigurable leaky wave antennas. The reconfigurable defected microstrip structure (RDMS) based phase shifter has demonstrated its capability to realize a compact phased antenna array for beamforming applications. The reconfigurable leaky wave antennas are capable of solving two disadvantages of traditional leaky wave antennas, including the narrow impedance bandwidth and frequency dependent beam scanning. This, in turn, makes the leaky wave antenna more promising for today's wireless communications systems.

Future work in this field includes the design of a RA that can deliver full reconfiguration of the three characteristics of the antenna. Such a RA can bring considerable benefits to many wireless communication systems. However, the strong linkage between an antenna's frequency response and its radiation characteristics makes it extremely challenging to independently control of operating frequency, polarization and radiation pattern. Therefore, new and effective techniques are needed to break the linkage in order to achieve full reconfiguration of an antenna. Another significant direction for future work is the reconfiguration of the entire radio frequency (RF) front-end as well as the signal processing in the physical layer. It is well known that antennas are only one part of the entire

transmitter and receiver sub-systems. If reconfigurable antennas are incorporated in wireless communications systems, the other parts of the system should also be capable of reconfiguring their characteristics in order to utilize the diversity derived from antenna agility. As research on these two topics progresses, RAs may play a major role to enhance the performance of the next-generation communications systems significantly.

References

Barrera JD, Huff GH (2014) A fluidic loading mechanism in a polarization reconfigurable antenna with a comparison to solid state approaches. IEEE Trans Antennas Propag 62:4008–4014

Bernhard JT (2005) Reconfigurable antennas. Wiley, New York

Bernhard JT, Volakis JL (2007) Antenna engineering handbook, 4th edn. McGraw-Hill, New York

Bernhard JT, Kiely E, Washington G (2001) A smart mechanically-actuated two-layer electromagnetically coupled microstrip antenna with variable frequency, bandwidth, and antenna gain. IEEE Trans Antennas Propag 49:597–601

Bhartia P, Bahl IJ (1982) Frequency agile microstrip antennas. Microw J :67–70

Cai Y, Guo YJ, Bird TS (2012) A frequency reconfigurable printed yagi-Uda dipole antenna for cognitive radio applications. IEEE Trans Antennas Propag 60:2905–2912

Chen RH, Row JS (2008) Single-fed microstrip patch antenna with switchable polarization. IEEE Trans Antennas Propag 56:922–926

Christodoulou CG, Tawk Y, Lane SA, Erwin SR (2012) Reconfigurable antennas for wireless and space applications. Proc IEEE 100:2250–2261

Davis ME (1975) Integrated diode phase-shifter elements for an X-band phased-array antenna. IEEE Trans Microw Theory Tech 23:1080–1084

Deal WR, Kaneda N, Sor J, Qian Y, Itoh T (2000) A new quasi-Yagi antenna for planar active antenna arrays. IEEE Trans Microw Theory Tech 48:910–918

Debogovic T, Perruisseau-Carrier J (2014) Array-fed partially reflective surface antenna with independent scanning and beamwidth dynamic control. IEEE Trans Antennas Propag 62:446–449

Ding C, Guo YJ, Qin PY, Bird TS, Yang Y (2014) A defected microstrip structure (DMS) based phase shifter and its application to beamforming antennas. IEEE Trans Antennas Propag 62:641–651

Ding C, Guo YJ, Qin PY, and Yang Y (2015) A compact phase shifter employing reconfigurable defected microstrip structure (RDMS) for phased array antennas. IEEE Trans. Antennas Propag

Donelli M, Azaro R, Fimognari L, Massa A (2007) A planar electronically reconfigurable Wi-Fi band antenna based on a parasitic microstrip structure. IEEE Antennas Wirel Propag Lett 6:623–626

Dorsey WM, Zaghloul AI (2009) Perturbed square-ring slot antenna with reconfigurable polarization. IEEE Antennas Wirel Propag Lett 8:603–606

Feresidis AP, Vardaxoglou JC (2001) High gain planar antenna using optimized partially reflective surfaces. IEE Proc Microw Antennas Propag 148:345–350

Feresidis AP, Goussetis G, Wang S, Vardaxoglou JC (2005) Artificial magnetic conductor surfaces and their application to low-profile high-gain planar antennas. IEEE Trans Antennas Propag 53:209–215

García-Vigueras M, Gómez-Tornero JL, Goussetis G, Weily AR, Guo YJ (2011) 1D-leaky wave antenna employing parallel-plate waveguide loaded with PRS and HIS. IEEE Trans Antennas Propag 59:3687–3694

Genovesi S, Candia AD, Monorchio A (2014) Compact and low profile frequency agile antenna for multistandard wireless communication systems. IEEE Trans Antennas Propag 62:1019–1026

Goldstone L, Oliner AA (1959) Leaky-wave antennas I: rectangular waveguides. IRE Trans Antennas Propag 7:307–319

Guzmán-Quirós R, Gómez-Tornero JL, Weily AR, Guo YJ (2012a) Electronically steerable 1D Fabry-Perot leaky-wave antenna employing tunable high impedance surface. IEEE Trans Antennas Propag 60:5046–5055

Guzmán-Quirós R, Gómez-Tornero JL, Weily AR, Guo YJ (2012b) Electronic full-space scanning with 1D Fabry-Pérot LWA using electromagnetic band gap. IEEE Antennas Wirel Propag Lett 11:1426–1429

Han SM, Kim CS, Ahn D, Itoh T (2005) Phase shifter with high phase shifts using defected ground structures. Electron Lett 41:196–197

Hansen RC (1998) Phased array antennas. Wiley, New York

Ho KM, Rebeiz GM (2014) A 0.9–1.5 GHz microstrip antenna with full polarization diversity and frequency agility. IEEE Trans. Antennas Propag 62:2398–2406

Horn RE, Jacobs H, Freibergs E, Klohn KL (1980) Electronic modulated beam steerable silicon waveguide array antenna. IEEE Trans Microw Theory Tech 28:647–653

Hsu SH, Chang K (2007) A novel reconfigurable microstrip antenna with switchable circular polarization. IEEE Antennas Wirel Propag Lett 6:160–162

Huang L, Chiao J, Lisio P (2000) An electronically switchable leaky wave antenna. IEEE Trans Antennas Propag 48:1769–1772

Huff GH, Feng J, Zhang S, Bernhard JT (2003) A novel radiation pattern and frequency reconfigurable single turn square spiral microstrip antenna. IEEE Microw Wirel Compon Lett 13:57–59

Hum SV, Xiong HY (2010) Analysis and design of a differentially-fed frequency agile microstrip patch antenna. IEEE Trans Antennas Propag 58:3122–3130

Hum SV, Okoniewski M, Davies RJ (2005) Realizing an electronically tunable reflectarray using varactor diode-tuned elements. IEEE Microw Wirel Compon Lett 15:422–424

Hum SV, Okoniewski M, Davies RJ (2007) Modeling and design of electronically tunable reflectarrays. IEEE Trans Antennas Propag 55:2200–2210

Ip A, Jackson DR (1990) Radiation from cylindrical leaky waves. IEEE Trans Antennas Propag 38:482–488

Jung CW, Lee M, Li GP, Flaviis FD (2006) Reconfigurable scan-beam single-arm spiral antenna integrated with RF-MEMS switches. IEEE Trans Antennas Propag 54:455–463

Khidre A, Lee KF, Yang F, Elsherbeni AZ (2013) Circular polarization reconfigurable wideband E-shaped patch antenna for wireless applications. IEEE Trans Antennas Propag 61:960–964

Lai MI, Wu TY, Wang JC, Wang CH, Jeng S (2008) Compact switched-beam antenna employing a four-element slot antenna array for digital home applications. IEEE Trans Antennas Propag 56:2929–2936

Li H, Xiong J, Yu Y, He S (2010a) A simple compact reconfigurable slot antenna with a very wide tuning range. IEEE Trans Antennas Propag 58:3725–3728

Li Y, Zhang Z, Chen W, Feng Z (2010b) Polarization reconfigurable slot antenna with a novel compact CPW-to-Slotline transition for WLAN application. IEEE Antennas Wirel Propag Lett 9:252–255

Li Y, Zhang Z, Zheng J, Feng Z, Iskander MF (2011) Experimental analysis of a wideband pattern diversity antenna with compact reconfigurable CPW-to-slotline transition feed. IEEE Trans Antennas Propag 59:4222–4228

Lim S, Ling H (2007) Design of electrically small pattern reconfigurable Yagi antenna. Electron Lett 43:1326–1327

Lim S, Caloz C, Itoh T (2005) Metamaterial-based electronically controlled transmission-line structure as a novel leaky-wave antenna with tunable radiation angle and beamwidth. IEEE Trans Microw Theory Tech 53:161–173

Liu L, Caloz C, Itoh T (2002) Dominant mode leaky-wave antenna with backfire-to-endfire scanning capability. Electron Lett 38:1414–1416

Lovat G, Burghignoli P, Jackson DR (2006) Fundamental properties and optimization of broadside radiation from uniform leaky-wave antennas. IEEE Trans Antennas Propag 54:1442–1452
Maheri H, Tsutsumi M, Kumagi N (1988) Experimental studies of magnetically scannable leaky-wave antennas having a corrugated ferrite slab/dielectric layer structure. IEEE Trans Antennas Propag 36:911–917
Martínez-Ros AJ, Gómez-Tornero JL, Goussetis G (2012a) Planar leaky-wave antenna with flexible control of the complex propagation constant. IEEE Trans Antennas Propag 60:1625–1630
Martínez-Ros AJ, Gómez-Tornero JL, and Goussetis G (2012b) Broadside radiation from radial arrays of substrate integrated leaky-wave antennas. In: Proceedings of the 6th European conference on antennas and propagation (EUCAP), pp 252–254
Nair SVS, Ammann MJ (2007) Reconfigurable antenna with elevation and azimuth beam switching. IEEE Antennas Wirel Propag Lett 9:367–370
Nikolaou S et al (2006) Pattern and frequency reconfigurable annular slot antenna using PIN diodes. IEEE Trans Antennas Propag 54:439–448
Parker D, Zimmermann DC (2002) Phased arrays – part I: theory and architecture. IEEE Trans Microw Theory Tech 50:688–698
Patil P, Khot UP, Bhujade S (2012) DGS based microstrip phase shifters. In: International conference on sensing technology, pp 723–728
Qin PY, Guo YJ, Liang CH (2010a) Effect of antenna polarization diversity on MIMO system capacity. IEEE Antennas Wirel Propag Lett 9:1092–1095
Qin PY, Weily AR, Guo YJ, Bird TS, Liang CH (2010b) Frequency reconfigurable quasi-Yagi folded dipole antenna. IEEE Trans Antennas Propag 58:2742–2747
Qin PY, Weily AR, Guo YJ, Liang CH (2010c) Polarization reconfigurable U-slot patch antenna. IEEE Trans Antennas Propag 58:3383–3388
Qin PY, Guo YJ, Cai Y, Dutkiewicz E, Liang CH (2011) A reconfigurable antenna with frequency and polarization agility. IEEE Antennas Wirel Propag Lett 10:1373–1376
Qin PY, Guo YJ, Weily AR, Liang CH (2012) A pattern reconfigurable U-slot antenna and its applications in MIMO systems. IEEE Trans Antennas Propag 60:516–528
Qin PY, Guo YJ, Ding C (2013a) A dual-band polarization reconfigurable antenna for WLAN systems. IEEE Trans Antennas Propag 61:5706–5713
Qin PY, Guo YJ, Ding C (2013b) A beaming steering pattern reconfigurable antenna. IEEE Trans Antennas Propag 61:4891–4899
Rodrigo D, Jofre L, Cetiner BA (2012) Circular beam-steering reconfigurable antenna with liquid metal parasitic. IEEE Trans Antennas Propag 60:1796–1802
Shafai C, Sharma SK, Shafai L, Chrusch DD (2004) Microstrip phase shifter using ground-plane reconfiguration. IEEE Trans Microw Theory Tech 52:144–153
Shelby RA, Smith DR, Shultz S (2001) Experimental verification of a negative index of refraction. Science 292:77–79
Sievenpiper DF (2005) Forward and backward leaky wave radiation with large effective aperture from an electronically tunable textured surface. IEEE Trans Microw Theory Tech 53:236–247
Sievenpiper D, Schaffner J, Lee JJ, Livingston S (2002) A steerable leaky-wave antenna using a tunable impedance ground plane. IEEE Antennas Wirel Propag Lett 1:179–182
Sung YJ, Jang TU, Kim YS (2004) A reconfigurable microstrip antenna for switchable polarization. IEEE Microw Wirel Compon Lett 14:534–536
Tawk Y, Costantine J, Avery K, Christodoulou CG (2011) Implementation of a cognitive radio front-end using rotatable controlled reconfigurable antennas. IEEE Trans Antennas Propag 59:1773–1778
Trentini GV (1956) Partially reflecting sheet arrays. IEEE Trans Antennas Propag 4:666–671
Veselago VG (1968) (Russian text 1967)) The electrodynamics of substances with simultaneously negative values of ε and μ. Sov Phys Usp 10:509–514
Wang S, Feresidis AP, Goussetis G, Vardaxoglou JC (2006) High-gain subwavelength resonant cavity antenna based on metamaterial ground planes. IEE Proc Microw Antennas Propag 153:1–6

Waterhouse R, Shuley N (1994) Full characterisation of varactor-loaded, probe-fed, rectangular, microstrip patch antennas. IEE Proc Microw Antennas Propag 141:367–373
Weily AR, Bird TS, Guo YJ (2008) A reconfigurable high gain partially reflecting surface antenna. IEEE Trans Antennas Propag 56:3382–3389
Whicker LR (1973) Review of ferrite phase shifter technology. IEEE MTT-S Int. Microwave Symp. Dig. 95–97
White JF (1974) Diode phase shifters for array antennas. IEEE Trans Microw Theory Tech 22:658–674
Wu SJ, Ma TG (2008) A wideband slotted bow-tie antenna with reconfigurable CPW-to-slotline transition for pattern diversity. IEEE Trans Antennas Propag 56:327–334
Xu F, Wu K (2005) Guided-wave and leakage characteristics of substrate integrated waveguide. IEEE Trans Microw Theory Tech 53:66–73
Yang SLS, Luk KM (2006) Design a wide-band L-probe patch antenna for pattern reconfigurable or diversity applications. IEEE Trans Antennas Propag 54:433–438
Yang XS, Wang BZ, Wu W, Xiao S (2007) Yagi patch antenna with dual-band and pattern reconfigurable characteristics. IEEE Antennas Wirel Propag Lett 6:168–171
Ye S, Wang XL, Wang WZ, Jin RH, Geng JP, Bird TS, Guo YJ (2012) High gain planar antenna arrays for mobile satellite communications. IEEE Antennas Propag Mag 54:256–268
Zhang S, Huff GH, Feng J, Bernhard JT (2004) A pattern reconfigurable microstrip parasitic array. IEEE Trans Antennas Propag 52:2773–2776